Universidade de Aveiro Departamento de Física
2013

ANA CLÁUDIA BERNARDES PARRACHO

PROCESSOS DE TRANSPORTE ASSOCIADOS A TROPOPAUSAS DUPLAS

TRANSPORT PROCESSES ASSOCIATED WITH DOUBLE TROPOPAUSES

Universidade de Aveiro Departamento de Física
2013

ANA CLÁUDIA BERNARDES PARRACHO

PROCESSOS DE TRANSPORTE ASSOCIADOS A TROPOPAUSAS DUPLAS

TRANSPORT PROCESSES ASSOCIATED WITH DOUBLE TROPOPAUSES

Dissertação apresentada à Universidade de Aveiro para cumprimento dos requisitos necessários à obtenção do grau de Mestre em Meteorologia e Oceanografia Física, realizada sob a orientação científica do Doutor José Manuel Henriques Castanheira, Professor Auxiliar do Departamento de Física da Universidade de Aveiro

Este trabalho é financiado por Fundos FEDER através do Programa Operacional Factores de Competitividade – COMPETE e por Fundos Nacionais através da FCT – Fundação para a Ciência e a Tecnologia no âmbito do projecto DYNOZONE (PTDC/CTE-ATM/105507/2008)

UNIÃO EUROPEIA
Fundo Europeu de Desenvolvimento Regional

COMPETE
PROGRAMA OPERACIONAL FACTORES DE COMPETITIVIDADE

FCT Fundação para a Ciência e a Tecnologia
MINISTÉRIO DA EDUCAÇÃO E CIÊNCIA

o júri / the jury

presidente /
president

Prof. Doutor Paulo Manuel Cruz Alves da Silva
professor auxiliar da Universidade de Aveiro

vogais /
examiners committee

Doutor Ricardo Machado Trigo
investigador auxiliar da Universidade de Lisboa

Prof. Doutor José Manuel Henriques Castanheira
professor auxiliar da Universidade de Aveiro

agradecimentos / acknowledgements

Gostaria de agradecer a todos os que me ajudaram a realizar esta dissertação, em especial ao Professor Doutor José Castanheira, pela orientação, ao Tiago Luna e Carlos Marques pela disponibilidade e pelo apoio informático prestado, e aos meus colegas, pelo apoio e troca de ideias proporcionada.

Gostaria ainda de agradecer à minha família, por todo o apoio dado ao longo dos anos.

Os dados analisados neste trabalho foram obtidos do projecto ERA-Interim do Centro Europeu de Previsão do Tempo a Médio Prazo (CEPTMP). Os campos ERA-Interim no formato utilizado para correr o modelo FLEXPART foram obtidos do CEPTMP e disponibilizados pelo Doutor Luis Gimeno da Facultade de Ciências de Ourense, Universidade de Vigo.

palavras-chave Tropopausa, tropopausa dupla, troposfera, estratosfera, intrusão, transporte, altura relativa, vorticidade potencial

resumo Este trabalho tem como objectivo estudar a origem dinâmica do ar que se encontra entre tropopausas duplas. Para o efeito, o modelo de dispersão lagrangiano FLEXPART foi corrido em modo de retro-trajectória, para dez dias, para todos os meses de Janeiro entre 1980 e 2010, para partículas lançadas duas vezes por dia entre tropopausas duplas, em locais selecionados. As trajectórias e vorticidades potenciais médias resultantes foram estudadas para eventos de tropopausa simples (ST) e de tropopausa dupla (DT), separadamente e os resultados foram comparados. Os resultados mostraram que, para eventos de DT, a altitude relativa e a vorticidade potencial nas trajectórias médias foram ambas inferiores em relação a eventos de ST. Também foi observado que as trajectórias que chegam às DTs tendem a ter origem em latitudes inferiores. Os resultados mostram que o transporte de ar subtropical e tropical em direcção ao pólo, acompanhado por intrusões troposféricas para a estratosfera extratropical, são mecanismos principais para a ocorrência de estruturas de tropopausas duplas.

keywords Tropopause, double tropopause, troposphere, stratosphere, intrusion, transport, relative altitude, potential vorticity

abstract This work aims to study the dynamic origin of the air that is found between double tropopauses. To do so, a Lagrangian dispersion model, FLEXPART was tested and run in backward mode for ten days, for every month of January between 1980 and 2010, for particles released twice a day between double tropopauses at selected sites. The resulting mean trajectories and potential vorticities were studied for single tropopause (ST) and double tropopause (DT) events separately and their results were compared. The results showed that, for DT events, the relative altitude and potential vorticity for the mean trajectories were both lower than for ST events, with a higher percentage of tropospheric particles in the DT cases. It was also observed that trajectories arriving between DTs tend to originate at lower latitudes. The results show that the poleward excursions of subtropical and tropical air accompanied by tropospheric intrusions into the lower extratropical stratosphere are a main mechanism for the occurrence of double tropopuase structures.

Contents

List of Figures

List of Tables

Symbols and Acronyms

DT – Double tropopause

ECMWF – European Centre for Medium-Range Weather Forecasts

ExTL – Extratropical Tropopause Layer

HIRDLS – High Resolution Dynamic Limb Sounder

MT – Multiple tropopause

PV – Potential vorticity

PVf – Fraction of particles with PV<2PVU

PVU – Potential vorticity units

ST – Single tropopause

STE – Stratosphere-troposphere exchange

TPf – Fraction of tropospheric particles

TTL – Tropical tropopause layer

z - Altitude

Z_{rel} – Relative altitude

WMO – World Meteorological Organization

Γ – Temperature lapse rate

λ - Longitude

φ - Latitude

Chapter 1. Introduction

The tropopause is a key feature of the atmosphere structure in midlatitudes (Hoskins et al., 1985) as well as in the tropics (Reid and Gage, 1996). It is defined as the boundary between the turbulently mixed troposphere and the more stable and stratified stratosphere. This transition layer is characterized by steep changes in lapse rate, potential vorticity (Hoskins et al., 1985) and chemical properties (Bethan et al., 1996). Although the tropopause may be operationally defined as a single level, it does not mark a discontinuity in the atmospheric properties. Rather, it is a level found in a layer where strong gradients of static stability and chemical mixing ratios occur. Therefore, it is extremely sensitive to variations in the thermal, dynamic and chemical structure of the atmosphere (Añel et al, 2008).

The height of the tropopause can be determined according to any of the aforementioned properties. In this work, the thermal definition of tropopause adopted by the World Meteorological Organization (WMO, 1957) is used, producing the lapse rate tropopause. The tropopause height varies with geographic location, both in latitude and longitude, due to synoptic and planetary waves and asymmetries in the tropical convection. However the variation with latitude is more accentuated. In the tropics, the tropopause is relatively high (approximately 16km), reflecting a transition between radiative-convective balance in the troposphere and radiative balance in the stratosphere (Thuburn and Craig, 2002). The extratropical tropopause is lower (between about 8 and 12km) with a complex structure determined by baroclinic wave dynamics (Held, 1982; Haynes et al., 2001; Schneider, 2004).

1.1 The thermal stratification and tropopause height

The thermal stratification and tropopause height of the extratropical atmosphere can be maintained by at least two mechanisms: convection and baroclinic eddies (Schneider et al., 2007). When the baroclinicity is small, convection is the dominant regime. In this case, radiative constraints, which are the balance between incoming and outgoing radiant energy fluxes in atmospheric columns, plus any dynamical energy flux divergences in the columns, determine the tropopause height. Conversely, if the baroclinicity is large enough, baroclinic entropy fluxes stabilize the thermal stratification and modify the tropopause height. In this case radiative constraints must be solved simultaneously with dynamical constraints. These express balance

conditions based on dynamical considerations, such as that moist convection maintains the thermal stratification close to a moist adiabat or that baroclinic eddy fluxes satisfy balance conditions derived from the mean entropy and zonal momentum balances.

In the simplest model of dynamical equilibrium in an atmospheric column, the dynamical constraint determines a constant tropospheric lapse rate and the radiative constraint determines the tropopause height that is consistent with the lapse rate and with a boundary condition, for example, a given surface temperature.

In addition, a third constraint is necessary to obtain a closed theory for the tropopause height, thermal stratification, and surface temperature. This third constraint is given by an energy balance condition at the surface, which determines the surface temperature given the differential heating of the surface and a theory of how the eddy flux of surface (potential) temperature depends on other mean-field quantities.

1.2 Multiple tropopauses and the importance of studying events of multiple tropopauses

Using the lapse rate definition of tropopause, the transition between the tropics and extratropics at a particular longitude is often characterized by a split in the tropopause, rather than a continuous transition (e.g. Kochanski, 1955). Over this region, it is possible to find, in a single sounding, multiple layers that fit the tropopause criteria (shown in Fig.1). The events in which this occurs are defined as multiple tropopause (MT) events. In the Northern Hemisphere, MT events have a maximum occurrence during the winter, over a well-defined latitudinal band between 30 and 40°N. Their maximum frequency is reported in zones of maximum cyclogenesis, coinciding with the subtropical jet stream and the occurrence of cutoff lows (Añel et al., 2007).

The behavior of the global tropopause (as well as the existence of double tropopauses) is related with stratosphere-troposphere exchange (STE). An overall understanding of STE is dependent on an ability to quantify tropopause (and double tropopause) structure and variability (e.g. Holton et al., 1995; Shepherd, 2002; Stohl et al., 2003).

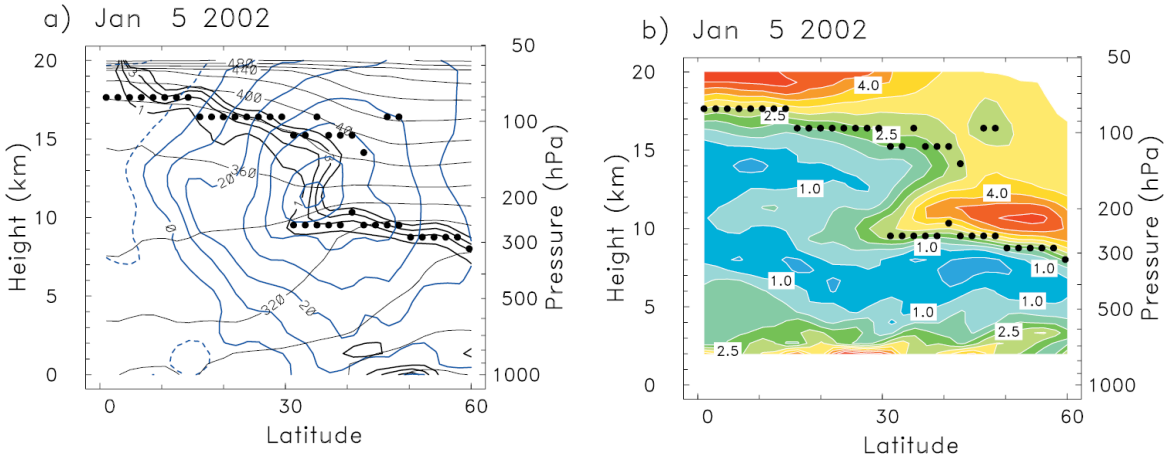

Fig. 1: (a) Height-latitude cross section of dynamical structure at 280°E derived from ERA40 data, including zonal winds (blue contours, m/s), isentropes (quasi-horizontal lines, contours at 20 K intervals), PV (heavy lines, contours of 1–4 PV units), and locations of the thermal tropopause (denoted by dots). (b) Corresponding static stability structure. Contours show Brunt-Väisälä frequency squared (N^2), with contour interval of $0.5\times10^4 s^{-2}$. Dots denote locations of the thermal tropopause (identical to (a)). Source: Randel et al., 2007.

The tropopause region has been identified as being of key importance for chemistry and climate. The Tropical Tropopause Layer (TTL) sets the chemical boundary condition for the stratosphere and its radiative balance plays an important role in the global energy balance. Whereas, the extra-tropical tropopause layer (ExTL) regulates the ozone budget, with potential impacts on surface chemistry (Gettelman et al., 2007). In addition, the tropopause, as a layer of strong increase of static stability, is important in the exchanges of trace constituents, momentum and energy between the troposphere and stratosphere. These exchanges play a role in the balance of stratospheric ozone, tropospheric pollution, global warming and may modulate the tropospheric climate in association with annular modes (Baldwin and Dunkerton, 1999, 2001; Thompson et al., 2002).

Dynamical diagnosis of both observations and model simulation indicates that variations in the zonally symmetric flow associated with the annular modes are forced by eddy fluxes in the free troposphere (Limpasuvan et al., 2000). In the Northern Hemisphere, stationary waves provide most of the eddy momentum fluxes and their behaviour can be partly explained with index of refraction arguments. When the tropospheric westerlies are displaced poleward, Rossby waves are refracted equatorward, inducing poleward momentum fluxes and reinforcing the high-latitude westerlies. In this case, the polar vortex is stronger because as planetary wave activity is refracted equatorward, it is less likely to propagate into the stratosphere and disturb the polar vortex.

However, in spite of the abundance of studies about multiple tropopauses events, significant uncertainty remains in many areas. Most notably, the origin of the air between tropopauses is still undetermined, and the mechanism leading to the formation and development of double tropopauses (DT) remains unknown. Several studies have pointed towards different (and sometimes opposing) explanations. A few of these studies' conclusions are presented henceforth.

1.3 Tropospheric origin of multiple tropopause events

Randel et al. (2007) studied and reported on the atmospheric structure of double tropopauses (the first step in understanding the mechanisms behind them) using radiosondes, ERA40 reanalysis, and GPS radio occultation temperature profiles. This particular study found that double tropopauses occur more frequently over midlatitude regions of both hemispheres, suggesting that the latitude band of frequent double tropopauses acts as a transition region between the tropics and extratropics. In addition, it was found that double tropopauses are more frequent above strong cyclonic circulation systems, and therefore are more common during winter. Finally, this study also found that double tropopauses are often linked to a poleward transport of tropical tropospheric air in the region above the subtropical jet core. Berthet et al. (2007) also suggest that these intrusions of tropospheric air may contribute to the ventilation of the lower stratosphere above the subtropical jet.

1.4 Does the air between tropopauses come from higher latitudes?

Wang and Polvani (2011) in a context of idealized baroclinic eddy life cycle experiment, found that large areas of double tropopauses form spontaneously at the nonlinear stage of the baroclinic life cycle evolution provided an extratropical tropopause inversion layer is present in the balanced initial temperature profile. In agreement with recorded observations, Wang and Polvani found that in their baroclinic life-cycle experiments, double tropopauses form predominantly in areas of cyclonic flow at upper levels. However, they found that the air masses that end up between the two tropopauses originate from high latitudes, which is not in agreement with results reported by other papers. This discrepancy suggests the existence of more than one mechanism in the advection of air masses between double tropopauses.

More recently, Añel et al. (2012) concluded that the source of the air masses between double tropopauses is mainly stratospheric, and air masses with tropospheric features are only present in a few cases.

1.5 Does the air between tropopauses come from the tropics?

Randel et al. (2007) found that measurements, from both balloons and satellites, of ozone profiles show systematically less ozone in the lower stratosphere during double tropopause events, in comparison with single tropopause cases. Taking into account other meteorological data, Randel et al. concluded that these ozone observations suggest that double tropopauses are regions of enhanced transport, from the tropics to higher latitudes above the subtropical jet cores.

Pan et al. (2009) examined two cases of subtropical tropospheric air intrusions into the lower stratosphere and related them with double tropopause events. They found that, in these cases, the secondary tropopause that extends from the subtropical tropopause break results from the transport of subtropical air into the high-latitude lower stratosphere. This was evidenced by the presence of a low-ozone, low-stability layer between tropopauses, which is characteristic of tropospheric air and is also characterized by relatively low potential vorticity values.

Castanheira et al. (2012) studied the statistical relationships between the occurrence of double tropopause events and the total column ozone and the lower stratospheric water vapor, using reanalyzed and satellite data. This study found a significant negative correlation between the area covered by double tropopauses and the total column ozone, as well as a negative correlation between the global area of tropopause events and water vapor in the lower stratosphere. They also found a large positive correlation between the areas covered by ozone laminae and double tropopause events as found in the High Resolution Dynamic Limb Sounder (HIRDLS) satellite dataset. Their results are consistent with a poleward displacement of tropical air within the upper troposphere/lower stratosphere region that may be accompanied by an increase in the frequency of tropospheric intrusions into the lower extratropical stratosphere, during double tropopause events.

In summary, no clear understanding exists of the origin of multiple tropopause events, yet. Possible explanations include the overlapping of the tropical and extratropical tropopause, or the folding of the tropopause linked to atmospheric circulation phenomena such as the cut-off low systems, the movement of jet-streams, or baroclinic waves.

1.6 Objectives and structure of this thesis

This work aims at studying the origin of the air between double tropopauses. It seeks to study the dynamic characteristics of double tropopauses and compare them with those of single tropopauses. The objective is to contribute to the understanding of the mechanisms responsible for the development of multiple tropopauses.

This was pursued by applying a Lagrangian particle dispersion model, FLEXPART, used to back-track particles released along the mid-latitudes in the northern hemisphere, at altitudes close to the tropopause (in the case of ST events) and between double tropopauses (in the case of DT events). The data and methods used to run the model and analyze its output are described in Chapter 2. The particles' positions and potential vorticity computed by the model were used to study the difference in origin of single and double tropopauses. These results are reported in Chapter 3. Finally, the conclusions of this work are exposed in Chapter 4.

Chapter 2. Methods and data

The Lagrangian particle dispersion model, FLEXPART version 8.2 (Stohl et al., 2005) was used in this work to compute back-trajectories that aim at studying the air found between double tropopauses. As a Lagrangian particle model, FLEXPART computes the trajectories of infinitesimally small air parcels, describing the transport and diffusion of tracers in the atmosphere. FLEXPART integrates the trajectory equation by using the zero acceleration scheme:

$$\boldsymbol{X}(t + \Delta t) = \boldsymbol{X}(t) + \boldsymbol{v}(\boldsymbol{X}, t)\Delta t \qquad (2.1)$$

which is accurate to the first order, to integrate the trajectory equation, with t being time, Δt the time increment, $\boldsymbol{X}$ the position vector and $\boldsymbol{v} = \overline{\boldsymbol{v}} + \boldsymbol{v_t} + \boldsymbol{v_m}$ the wind vector that is composed of the grid scale wind $\overline{\boldsymbol{v}}$, the turbulent wind $\boldsymbol{v_t}$ and the mesoscale wind fluctuations $\boldsymbol{v_m}$. In this study, the grid scale wind $\overline{\boldsymbol{v}}$ was provided by the ERA-interim reanalysis from the European Centre for Medium-Range Weather Forecasts (ECMWF).

2.1 Changes to the tropopause calculation

The model's routine for calculating tropopause height (calcpar.f, in the FLEXPART package) was changed in order to conform to the WMO lapse-rate criterion (WMO, 1957), as follows.

1) The first tropopause is defined as the lowest level at which the lapse rate decreases to 2°C/km or less, provided also the average lapse rate between this level and all higher levels within 2 km does not exceed 2°C/km.

2) If above the first tropopause the average lapse rate between any level and all higher levels within 1 km exceeds 3°C/km then a second tropopause is defined by the same criterion as under (1). This tropopause may be either within or above the 1 km layer.

This definition was implemented by the following algorithm, similar to the method described by Reichler (2003), but using an altitude coordinate instead of pressure.

Let T_1, T_2, … T_n be the temperature at the ECMWF model levels altitudes z_1, z_2, … z_n. The lapse rate,

$$\Gamma(z) = -\frac{\partial T}{\partial z}, \qquad (2.2)$$

is calculated at the half levels

$$z_{i+1/2} = \frac{z_i + z_{i+1}}{2} \tag{2.3}$$

using the finite difference formula

$$\Gamma_{i+1/2} = \frac{T_i - T_{i+1}}{z_{i+1} - z_i} \tag{2.4}$$

The temperature at half levels is estimate by linear interpolation

$$T_{i+1/2} = \frac{T_i + T_{i+1}}{2} \tag{2.5}$$

Starting at a full level z_i just above 5km, in order to avoid inversions in the lower troposphere, we search for the half level $z_{j+1/2}$ where $\Gamma_{j+1/2}$ is smaller than the critical lapse rate, $\Gamma_{tp} = 2K/km$ for the first time. A candidate tropopause level, z_{tp} , is determined by linear interpolation onto Γ

$$z_{tp} = \frac{z_{j+1/2} - z_{j-1/2}}{\Gamma_{j+1/2} - \Gamma_{j-1/2}} (\Gamma_{tp} - \Gamma_{j-1/2}) + z_{j-1/2} \tag{2.6}$$

and the temperature T_{tp} at the level z_{tp} is also estimated by linear interpolation onto z

$$T_{tp} = \frac{T_{j+1/2} - T_{j-1/2}}{z_{j+1/2} - z_{j-1/2}} (z_{tp} - z_{j-1/2}) + T_{j-1/2} \tag{2.7}$$

Next, the first level z_k which is at least 2 km above z_{tp} is identified, and the average lapse rates between the estimated level z_{tp} and each one of the higher full levels within layer (z_{tp}, z_k) are then checked to determine if they remain below the critical lapse rate, $\Gamma_{tp} = 2K/km$. If the mean lapse rates of all levels verify that condition, the height z_{tp} is taken as the level of the tropopause. If there is a level within (z_{tp}, z_k) whose average lapse rate is higher than the critical lapse rate, a new search for the tropopause level starts at the full level z_{j+1} to find a new candidate level z_{tp} and an associated temperature T_{tp} for the tropopause. The process is repeated until a pair (z_{tp}, T_{tp}) which satisfies the above conditions is found. It is important to note that the mean lapse rate criterion here applied is more restrictive than simply requiring that the (single) mean lapse rate between the levels z_{tp} and z_k remains below the critical lapse rate, as done by the initial version of the routine calcpar.f available in the FLEXPART package. Reichler et al. (2003) seem to apply the less restrictive criterion. On the other hand, Birner (2010) applied the more restrictive thickness criterion and showed higher sensitivity of the tropopause altitude to the way the thickness criterion is applied, in the subtropical region where DT events occur frequently.

2.2 Single and double tropopauses dataset

Using the temperature profiles from ERA-Interim reanalysis on isobaric levels with a horizontal resolution of 1.5°lat. x 1.5°long., the pressure and temperature of the first and second (when it existed) tropopauses were calculated twice a day (00 and 12 UT), for January and December, from 1979 to 2010. The tropopauses were computed using an algorithm similar to that used by Reichler et al. (2003) but with the thickness as described in the previous section. As in Reichler *et al.*, the lapse rate was calculated using the formula

$$\Gamma(p) = -\frac{\partial T}{\partial z} = \frac{\partial T}{\partial p^k}\frac{p^k}{T}\left(\frac{k\ g}{R}\right) \tag{2.8}$$

with T temperature, p pressure, and $k = {}^{R}/_{c_p}$, where R and c_p denote the specific gas constant and the specific heat capacity at constant pressure for dry air, respectively. The finite difference approximation this equation is

$$\Gamma_{i+1/2} = \frac{(T_{i+1} - T_i)}{(p_{i+1}^k - p_i^k)}\frac{(p_{i+1}^k + p_i^k)}{(T_{i+1} + T_i)}\left(\frac{k\ g}{R}\right) \tag{2.9}$$

where

$$\Delta z_i = -\left(\frac{R}{k\ g}\right)\frac{(T_{i+1} + T_i)}{(p_{i+1}^k + p_i^k)}(p_{i+1}^k - p_i^k) \tag{2.10}$$

is the thickness between two consecutive isobaric levels.

The temperature of the tropopauses was determined by linear interpolation on p^k. Castanheira and Gimeno (2011) have applied this algorithm to diagnose double tropopauses, but with the second condition in the WMO definition of lapse rate tropopause reduced to 2.5 K/km.

The altitudes of the tropopauses were determined by linear interpolation of geopotential height on $\log p$ and using the temperature of the tropopause for the definition of the scale height factor. Castanheira and Gimeno (2011) have applied this algorithm to find multiple tropopauses.

Single and double tropopauses variables obtained by these calculations were used in the configuration of FLEXPART runs and in the definitions of single tropopause events (STs) and double tropopause events (DTs) , as described in the following sections.

2.3 Input data and model configuration

FLEXPART was run off-line, in the backward mode (developed by Flesch et al. (1995) and Seibert and Frank (2004)) using the following ERA-Interim meteorological fields (six-hourly reanalysis, at 00, 06, 12 and 18UTC, plus 3-hour forecasts, at 03, 09, 15 and 21UTC, in order to have three-hourly input data, with 1°x1° resolution at 60 model hybrid levels):

- Two-dimensional fields: surface-pressure, total cloud cover, 10m horizontal wind components, 2m temperature and dew point temperature, large-scale and convective precipitation, sensible heat flux, east/west and north/south surface stress, topography, land-sea mask and standard deviation of topography.
- Three-dimensional fields: horizontal and vertical wind components, temperature and specific humidity, defined at hybrid ECMWF model levels.

Ten-day back trajectories were computed twice a day (with six-hour release time intervals centered on 00 and 12UTC), for every month of January, between 1980 and 2010. The month of January was chosen because it is a cold season month, and during this season double tropopauses are more frequent in the northern hemisphere. The temporal domain used in the trajectory computation was 10 days because the duration of the stronger double tropopause structures are found to vary between 3 and 12 days (Peevey et al., 2012). Therefore, we hope that most of the back-trajectories ending between double tropopauses started in a region with a single tropopause.

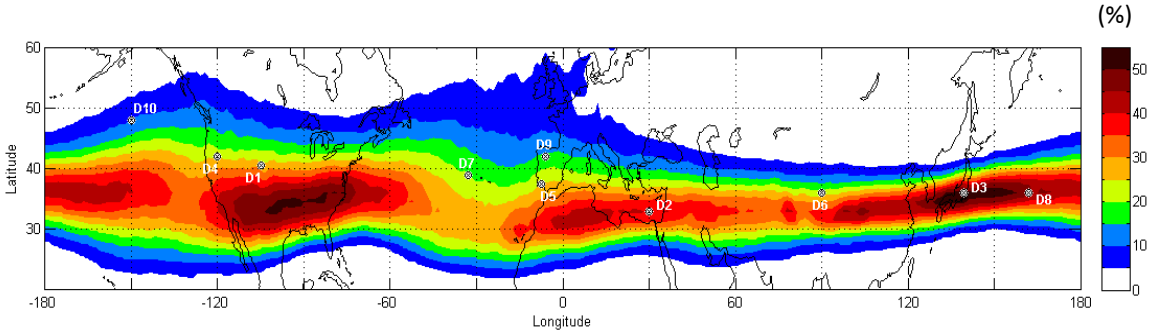

Fig. 2: Frequency of DT events for January (in %) overlaid with the domains used in this study (dots). Domains 2, 3 and 8 were chosen for their location in relatively high frequency of DT events in January. Domains 1, 4, 5, 6 and 7 were chosen for their location in medium frequency regions. Domains 9 and 10 are located in regions of relatively low frequency of DT events.

Particles (2000 for each release) were released from ten small domains (three-dimensional boxes) along the Northern Hemisphere mid-latitudes (as shown in Fig. 2 and Table 1). These domains were chosen in order to have regions of high, medium and low frequency of DT events (Fig. 2).

Table 1: Coordinates used to define domains 1 through 10.

Domain	Lat_S (°N)	Lat_C (°N)	Lat_N (°N)	Lon_W (°E)	Lon_C (°E)	Lon_E (°E)
D1	39.75	40.50	41.25	-105.75	-105.00	-104.25
D2	32.25	33.00	33.75	29.25	30.00	30.75
D3	35.25	36.00	36.75	138.75	139.50	140.25
D4	41.25	42.00	42.75	-120.75	-120.00	-119.25
D5	36.75	37.50	38.25	-8.25	-7.50	-6.75
D6	35.25	36.00	36.75	89.25	90.00	90.75
D7	38.25	39.00	39.75	-33.75	-33.00	-32.25
D8	35.25	36.00	36.75	161.25	162.00	162.75
D9	41.25	42.00	42.75	-6.75	-6.00	-5.25
D10	47.25	48.00	48.75	-150.75	-150.00	-149.25

To ensure that most particles were released between tropopauses (in the case of DT events), the domains' vertical boundaries (Z_1 and Z_2) were defined for each January, using the following criteria:

$$Z_1 = \overline{z_{TP1}} + 2\sigma_{TP1} \quad (2.11a)$$

$$Z_2 = \overline{z_{TP2}} - \sigma_{TP2} \quad (2.11b)$$

In which $\overline{z_{TP}}$ is the mean tropopause height for the first and second tropopauses (1 and 2, respectively) and σ_{TP} is its standard deviation, both computed for each January. In 2.11a, we chose the lower boundary, Z_1, to be 2σ above the mean height of the first tropopause in order to exclude the extratropical stratospheric air that must lie just above the first tropopause (as seen in Fig. 1, in Chapter 1).

2.4 Model output

The model's output was obtained three-hourly and the plume centroid trajectory, which is the mean position of the particles at each instant, was computed for each release site (Dorling et al.,

1992 and Stohl et al., 2002). This study was focused on the analysis of the following model output variables:

- Plume centroid coordinates, x and y, which are the longitude and latitude (respectively) of the center of mass of the particles released, at each instant;
- Average height of particles, z, at each instant;
- Tropopause height, which is the mean tropopause height at the position of particles, at each instant;
- Potential vorticity, which is the mean Ertel potential vorticity for all particles, at each instant. The Ertel potential vorticity is defined as:

$$PV = \frac{1}{\rho}\boldsymbol{\zeta_a} \cdot \boldsymbol{\nabla}\theta \tag{2.12a}$$

where θ is the potential temperature, ρ is the fluid density and $\boldsymbol{\zeta_a}$ is the absolute vorticity, and is defined as:

$$\boldsymbol{\zeta_a} = 2\boldsymbol{\Omega} + \boldsymbol{\zeta} \tag{2.12b}$$

in which:

$$\boldsymbol{\zeta} = \boldsymbol{\nabla} \times \boldsymbol{u} \tag{2.12c}$$

Is the relative vorticity, $\boldsymbol{\Omega}$ is the angular velocity, $\boldsymbol{\nabla}$ is the three-dimensional gradient operator, and u is the three-dimensional velocity.

The potential vorticity, as defined by this equation is conserved following the motion for adiabatic, frictionless flow.

- Fraction of particles residing in the troposphere, using both the thermal lapse rate and the dynamical definitions of tropopause. In the first case, the fraction of particles below the tropopause at the position of the particles is computed, and in the second case, the fraction of particles with potential vorticity below 2PVU is calculated.

2.5 Separating DT and ST events

Using the first and second tropopause heights computed using ERA Interim data (used previously to define the vertical boundaries of the domains), particle arrival times (*t*) were separated into ST and DT events, according to the following procedure.

Single Tropopause events, for a domain *Di*, were determined using the following conditions:

1. The thermal profiles at the central point of the (arrival) domain *Di*, as well as at the 4 grid points defining its edges, have single thermal tropopauses, at an instant, *t*;

2. Let $h_{5ST}(t,n)$ be the mean height of the single tropopauses in these five points, at the *t* instant of the *n* year, and let $M_{h5ST}(n)$ and $\sigma_{h5ST}(n)$ be the mean and standard deviation of h_{5ST} at the *n* year. In order for *t* to be considered an ST event, for a domain *Di*, the following condition must be met:

$$M_{h5ST}(n) - 2\sigma_{h5ST}(n) \leq h_{5ST}(t,n) \leq h_1(n,Di) \quad (2.13)$$

In which h_1 is the lower boundary of *Di* at the *n* year. This condition will ensure that only cases where the height of the first tropopause is below the lower boundary of *Di* were considered. The minimum threshold ($M_{h5ST}(n) - 2\sigma_{h5ST}(n)$) excludes events that may be due to an erroneous identification of the tropopause.

Double Tropopause events must verify the following conditions:

1. The thermal profiles at the central point of the (arrival) domain *Di* as well as at the 4 grid points defining its edges have multiple thermal tropopauses, at the *t* instant;

2. If $h_{5DT1}(t,n)$ is the mean height of the first tropopause in these five points, at the *t* instant of the *n* year, and $M_{h5DT1}(n)$ and $\sigma_{h5DT1}(n)$ are the mean and standard deviation of h_{5DT1} at the *n* year. The following condition must be confirmed for *Di*:

$$M_{h5DT1}(n) - 2\sigma_{h5DT1}(n) \leq h_{5DT1}(t,n) \leq h_1(n,Di) \quad (2.14a)$$

3. Let $h_{5DT2}(t,n)$ be the mean height of the second tropopause in those five points, at the *t* instant of the *n* year, and let $M_{h5DT2}(n)$ and $\sigma_{h5DT2}(n)$ be the mean and standard deviation of h_{5DT2} at the *n* year, respectively. The following condition must be confirmed for *Di*:

$$M_{h5DT2}(n) + 2\sigma_{h5DT2}(n) \geq h_{5DT2}(t,n) \geq h_2(n,Di) \quad (2.14b)$$

In which h_2 is the upper boundary of *Di* at the *n* year. This condition will ensure that only cases where the height of the second tropopause is above the upper boundary of *Di* were considered. The maximum threshold ($M_{h5DT2}(n) + 2\sigma_{h5DT2}(n)$) excludes events that may be due to an erroneous identification of the second tropopause.

In the calculation of some statistics, an additional condition that the nearest point within the trajectory was not a double tropopause was also implemented, in order to exclude portions of the trajectories where double tropopauses were already present.

2.6 Trajectories

Back-trajectories were computed by FLEXPART for each release date. We analyze the plume centroid trajectory using tropopause relative altitude coordinates ($\lambda, \varphi, Z_{rel}$), where λ and φ are the longitude and the latitude, respectively. The coordinate Z_{rel} is the altitude relative to the tropopause given by:

$$Z_{rel} = z_c - z_{TP} \tag{2.15}$$

where z_c is the altitude of the plume centroid trajectory, at a given instant, and z_{TP} is the mean altitude of the first lapse rate tropopause at the position of particles, at the same instant. Therefore, Z_{rel} is the mean of the relative altitude of all particles, in relation to the tropopause, at their corresponding horizontal positions.

In order to compute the trajectory distributions for ST and DT events, small 1°x1° bins were defined covering the entire northern hemisphere. The number of times a (segment of a) trajectory fell on each bin was counted. The number of times a bin was crossed by a trajectory was divided by the total number of ST or DT events (which varied with each domain), allowing for empirical estimates of the spatial probability density functions of trajectories for both ST and DT cases. In order to compare the trajectory distributions in ST and DT cases, the difference fields between trajectory densities for DT and ST events were computed.

Using the empirical estimates of the spatial probability density functions,$f_h(\lambda, \varphi)$, the average latitude, $\bar{\varphi}$, of the trajectories at a longitude λ was calculated using the following formula.

$$\overline{\varphi(\lambda)} = \sum_{i=1}^{N_{lat}} \frac{f_h(\lambda, \varphi)\, \varphi}{f_h(\lambda, \varphi)} \tag{2.16a}$$

The same analysis was used to study the vertical component of the trajectories. In this case, 250m in Z_{rel} by 3° in longitude bins were defined and the number of times a segment of trajectory fell on each bin was counted. The number of times a bin was crossed by a trajectory was divided by the total number of ST or DT events, resulting in empirical estimates of the spatial probability density

functions of relative altitude in longitude, for both ST and DT cases. The difference fields between DT and ST events were computed and the average relative altitude, $\overline{Z_{rel}}$, at a longitude λ was calculated using the following formula.

$$\overline{Z_{rel}}(\lambda) = \sum_{i=1}^{N_{lat}} \frac{f_v(\lambda, Z_{rel})\, Z_{rel}}{f_v(\lambda, Z_{rel})} \tag{2.16b}$$

Finally, this analysis was also used for the mean potential vorticity. In this case, bins of 0.2PVU by 3° in longitude were established and the number of times a segment of trajectory fell on each bin was counted. Again, the number of times a bin was crossed by a trajectory was divided by the total number of ST or DT events, resulting in empirical estimates of the spatial probability density functions of potential vorticity in longitude, for both ST and DT cases. The difference fields between DT and ST events were computed and the average potential vorticity, $\overline{PV}$, at a longitude λ was calculated using the following formula.

$$\overline{PV}(\lambda) = \sum_{i=1}^{N_{lat}} \frac{f_{PV}(\lambda, PV)\, PV}{f_{PV}(\lambda, PV)} \tag{2.16c}$$

Because for each ST or DT event, the back-trajectories were recorded at eighty instants (10 days times eight 3-hour intervals), the ratio of the number of times a bin was crossed by a trajectory to the total number of ST or DT events produces estimates of the probability density functions, f_v , f_h and f_{PV}, normalized to 80. For 5-day back-trajectories the estimated the probability density functions will be normalized to 40.

2.7 Temperature profiles

Using six-hourly ERA-Interim meteorological fields, temperature profiles were computed for the month of January, using a tropopause-based averaging (Birner, 2006). This method of averaging uses the tropopause as a common reference level for all vertical profiles within the mean, so that if $T(t, z)$ is the temperature with respect to sea level, and $z_{TP}(t)$ is the tropopause height at time-instant t, then $\overline{T(t, z - z_{TP}(t))}$ is its tropopause-based time-average. Once the latter has been calculated, the vertical coordinate is readjusted using the time-averaged altitude of the tropopause, $\overline{z_{TP}}$, using:

$$\bar{z} \equiv z - z_{TP} + \overline{z_{TP}} \tag{2.17}$$

This averaging method uncovers the strong inversion at the tropopause in the mean vertical temperature gradient, that exists on average throughout the extratropics, and which conventional averages are not capable of capturing.

Chapter 3. Results and discussion

Part 1. Test cases

In order to test the model's sensitivity to double tropopauses and their indicators, test cases were run, based on double tropopause events observed and recorded in literature. These test cases were analyzed to confirm that the recorded features observed in measured double tropopauses were represented by the model. These features, reported by the experimental cases, include a decrease in potential vorticity between tropopauses, with an increasing fraction of particles with a potential vorticity lower than 2PVU. Also expected is an increase of tropospheric particles (i.e. particles with Z_{rel}<0) ending between double tropopauses and in particle trajectories with a southerly component.

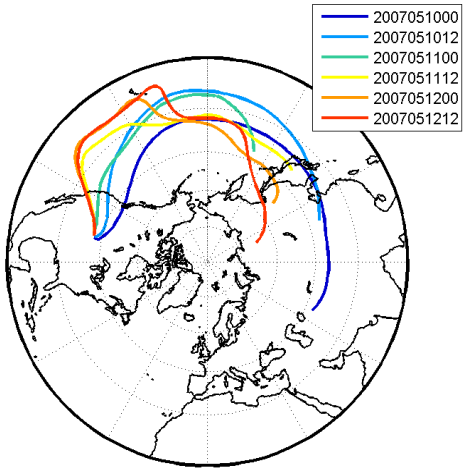

Fig. 3: Ten-day back-trajectories for particles arriving at a small domain over North America from the 10th to the 12th of May 2007.

was first developed off the west coast of North America, along the jet stream. It then moved into the continent, covering more than 20° in latitude. Measured ozone cross sections and potential temperature lapse rates showed that a layer of low-ozone and low-stability air extended into higher latitudes from the subtropics. In

3.1.1 Event of 11th of May 2007

According to Pan et al. (2009), a large intrusion event was observed by the High Resolution Dynamic Limb Sounder (HIRDLS) instrument over North America between the 8th and the 13th of May 2007 (peaking on the 11th of May). Reports indicate that the event

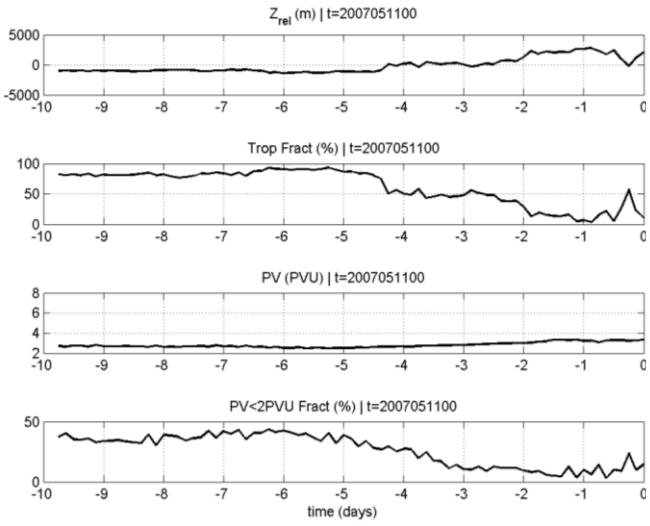

Fig. 4: Time-series for (t-b) Zrel, Trop Fract, PV and PV<2 PVU Fract for trajectories ending on the 11th of May of 2007, at 00UTC and arriving at a 1.5x1.5° box centered at 42°N and 102°W.

addition to low ozone, low potential vorticity (less than 6PVU) was also reported between double tropopauses, suggesting tropospheric influence in this region.

This is consistent with model results (Fig. 3) where ten-day back-trajectories of particles arriving at a 1.5°x1.5° box centered at 42°N and 102°W between double tropopauses have a southerly origin (especially for less than five days backward from the 12th of May and for over five days backward from the 10th of May). This is in accordance with the results obtained for plume trajectories for the 11th of May at 00UTC (Fig. 4), in which relative altitudes (Z_{rel}) were negative during the five days and more prior to arrival and potential vorticity (PV) is low (between 2 and 4PVU). Furthermore, the fraction of tropospheric particles is close to one hundred percent and the fraction of particles with PV<2PVU is close to fifty percent, during the same period.

3.1.2 Event of 11th of April 2007

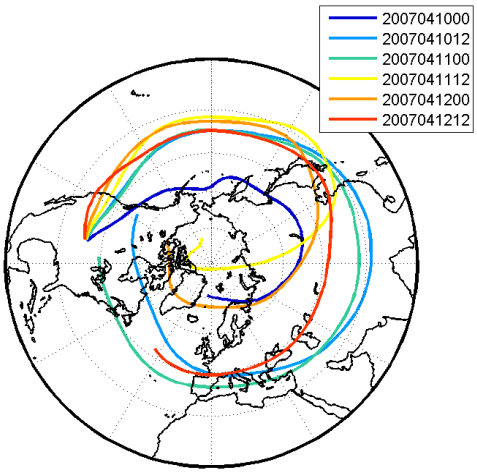

Fig. 5: Ten-day back-trajectories for particles arriving at a small domain over North America from the 10th to the 12th of April 2007.

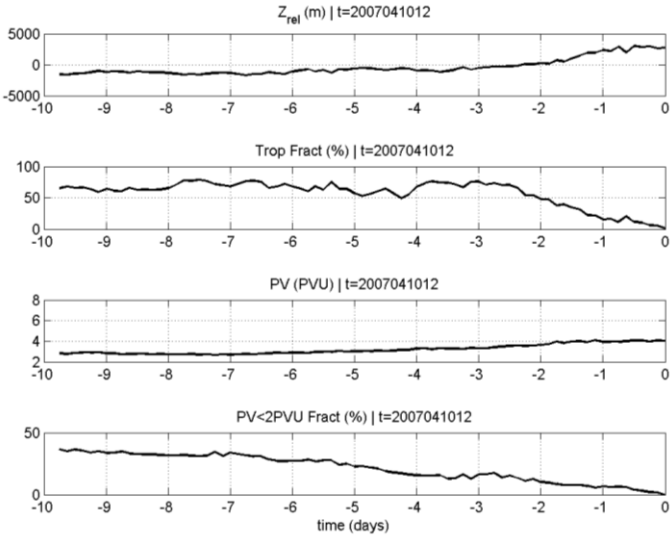

Fig. 6: Time-series for (t-b) Zrel, Trop Fract, PV and PV<2 PVU Fract for trajectories ending on the 10th of April of 2007, at 12UTC and arriving at a 1.5x1.5° box centered at 39°N and 99°W.

Pan et al. (2009) also reported a case observed around the 11th of April 2007. In this case, as in the case before, plume trajectories, especially in the two days and over leading up to the 10th to 12th of April, are southerly (Fig. 5). This is particularly visible for the 10th of April, at 12UTC. At this instant, the majority of particles between tropopauses is of tropospheric origin, with corresponding negative relative altitudes and relatively small values of potential vorticity (Fig. 6).

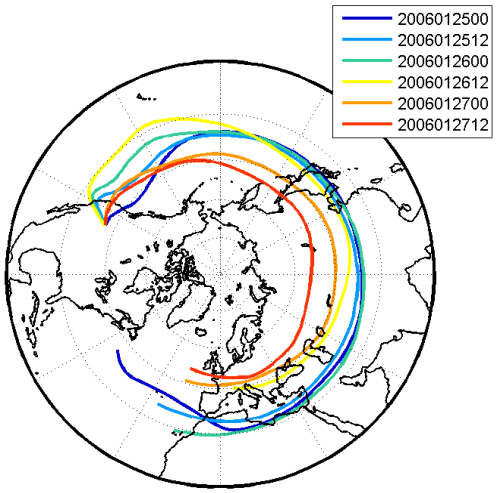

Fig. 7: Ten-day back-trajectories for particles arriving at a small domain over North America from the 25th to the 27th of January 2006.

(green and yellow lines in Fig. 7). Also, results suggest that the air between double tropopauses, in this case, comes from the lower stratosphere, as evidenced by the low but positive relative altitudes of the plume trajectories ending at this date (Fig. 8). Still, the fraction of tropospheric particles for the seven days and over preceding the 26th of January reaches up to 40 percent and the potential vorticity remains low (between 4 and 6PVU) with a small percentage of particles with PV<2PVU.

3.1.3 Event of 26th of January 2006

According to Olsen et al. (2008), on the 26th of January 2006, the HIRDLS observed low mixing ratios of ozone near 100hPa over North America. The evolution of the layer was studied using the Global Modeling Initiative model (with HIRDLS observations). The reported results suggested that the air in this layer had been transported through isentropic poleward advection from the lower tropical stratosphere. This is observed in the results produced by the model used in this work, in which plume trajectories are decidedly poleward in the hours/ days preceding the 26th of January 2006

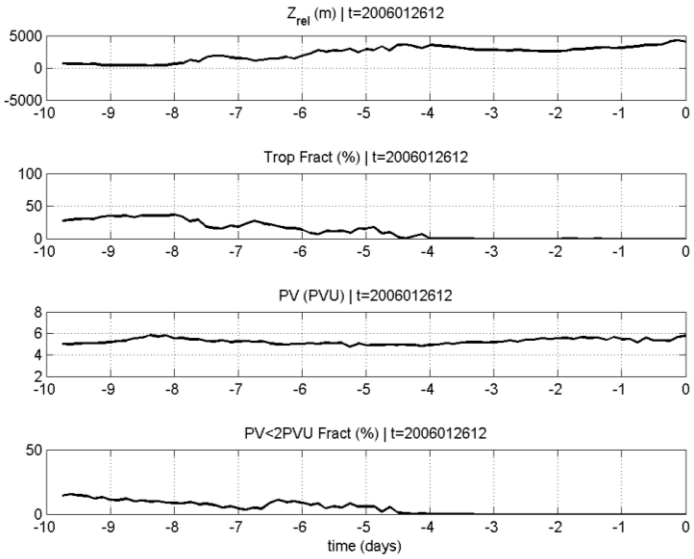

Fig. 8: Time-series for (t-b) Zrel, Trop Fract, PV and PV<2 PVU Fract for trajectories ending on the 26th of January of 2006, at 12UTC and arriving at a 1.5x1.5° box centered at 42°N and 111°W.

3.1.4 Concluding remarks

In conclusion, the results obtained for these tests cases suggest that FLEXPART integrations are sensitive to the occurrence of double tropopause events. The model was able to simulate the

measured characteristics (trajectories, relative altitudes and potential vorticity) associated with upper tropospheric and lower stratospheric intrusions, reported in literature.

As such, the model will be used in the second part of this work to study the climatological origin of air between double tropopauses, using ten-day, backward model runs for every January between 1980 and 2010, for several selected locations. The results are presented and analyzed in the next section.

Part 2. Model runs for 1980-2010

3.2.1 Trajectories

Firstly, five-day back-trajectory empirical probability distributions were calculated for each domain, for DT and ST events separately. The differences in probability fields between DT and ST events are presented in Fig. 9-15. Positive (red) values are observed where there is a predominance of trajectories of DT events and negative (blue) values occur when ST trajectories are dominant. Although it is not shown, the difference fields are of the same order as the separate fields for the DT and ST events. In addition, mean latitudes, mean relative altitudes and mean potential vorticities for each degree of longitude were computed and plotted as red (DT) and blue (ST) lines. A longitude interval was set, with mean latitudes for ST and DT events spanning the same longitudes.

The horizontal projections of the centroid trajectories show that for each domain at study, the air that is found between double tropopauses comes, on average, from lower latitudes than the air found in the respective domains for single tropopause cases. Accordingly, the average latitude for DT events is lower than the average latitude observed in ST events, with differences between mean latitudes in DT and ST cases reaching up to 15° (in D5, for instance).

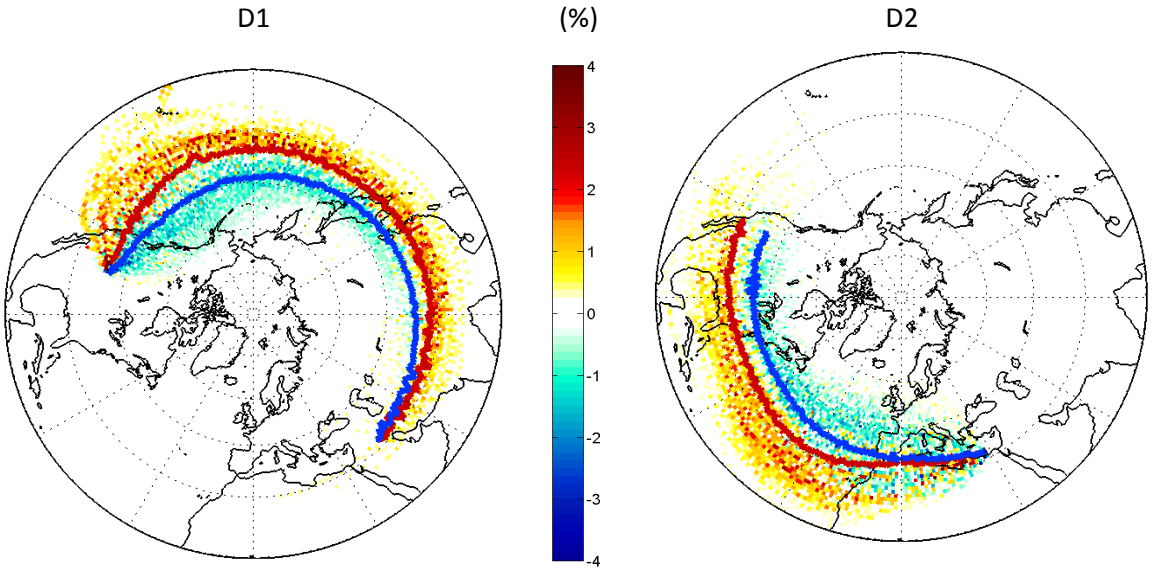

Fig. 9: DT-ST difference between the five-day back-trajectory probability distribution, between 1980 and 2010, for the first domain, D1 (left) and the second domain, D2 (right). Overlaid is the average latitude of trajectories for each longitude interval, in red and blue lines for DT and ST events, respectively.

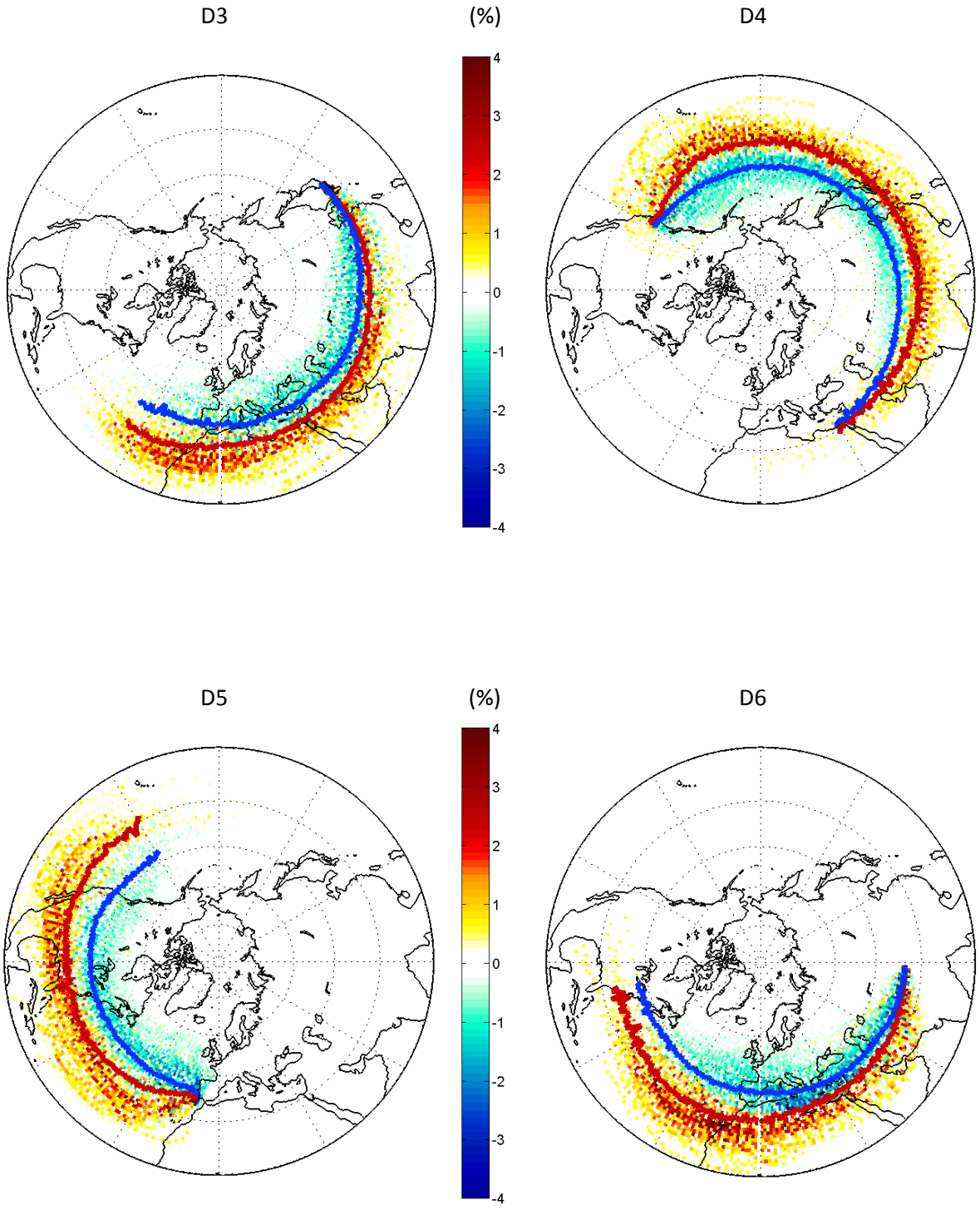

Fig. 10: As in Fig. 9, but for domains D3 through D6.

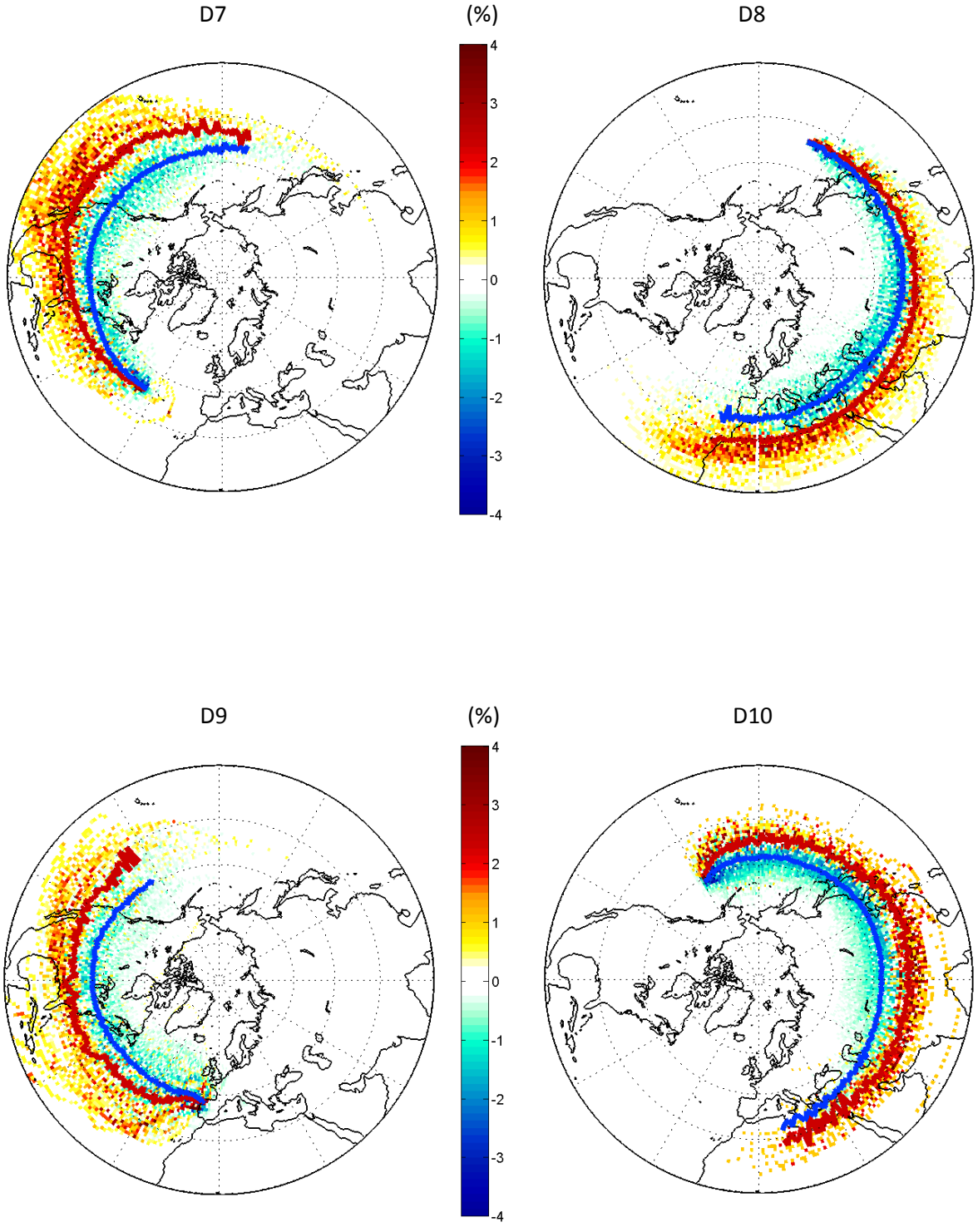

Fig. 11: As in Fig. 9, but for domains D7 through D10.

Even though in every domain at study the mean latitude for DT events is lower than the mean latitude for ST events, there are some noteworthy differences between some of the domains, namely:

- For domains 1, 4 and 7, mean latitudes for ST and DT events tend to converge as longitudes move away from the source point. This indicates that, for around 5 days and beyond, there is no preferential latitude for the particles' position. On the other hand, for domains 2, 3, 5, 8 and 9, the mean latitudes tend to diverge, with mean latitudes for DT events becoming more distant from those of ST events for increasing backwards time.
- For most cases, mean trajectories for DT and ST events diverge directly from the source point. However, in the case of domains 2, 3 and 8 the two mean trajectories almost overlap close to their source. This is especially visible in the case of D2, in which mean trajectories for ST and DT events overlap for about 30° of longitude. In this case, negative trajectory density differences are observed in relatively lower latitudes, as well. This could be because double tropopauses might have already been present at these longitudes.

In summary, air between double tropopauses originates mostly from lower latitudes than the air found at the same altitudes for single tropopauses. This is consistent with results reported by Randel et al. (2007) and Pan et al. (2009), and with the hypothesis that a frequent mechanism for DT events are related with the tropospheric intrusion caused by the overlapping of the higher tropical tropopause over the lower extra tropical tropopause.

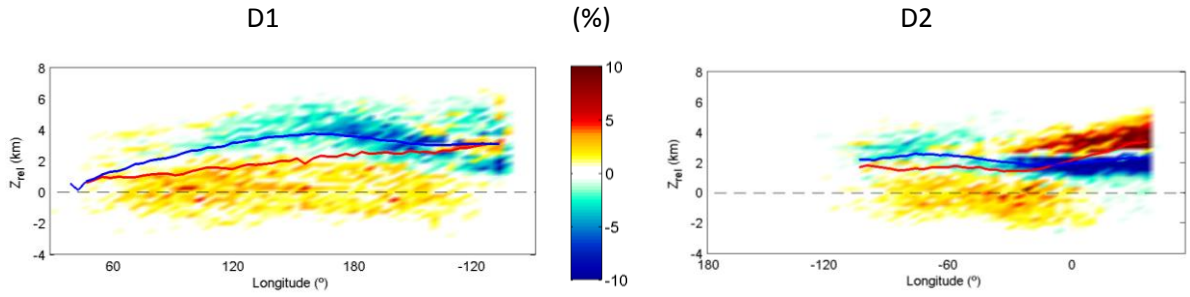

Fig. 12: DT-ST difference between the five-day back-trajectory Z_{rel} probability distribution, between 1980 and 2010, for the first domain, D1 (left) and the second domain, D2 (right). Overlaid is the average Z_{rel} of trajectories for each longitude interval, in red and blue lines for DT and ST events, respectively.

Next, the altitude-longitude projections of the computed trajectories were analyzed, using the mean relative altitude of the centroid trajectory (in relation to the tropopause computed by the model), Z_{rel}. This was done to see if for DT events mean trajectories originated at lower relative

altitudes. The five-day back-trajectory empirical probability distributions were computed for Z_{rel}, for DT and ST events and the difference between them was plotted and is shown in Fig. 12 -13. Mean Z_{rel} for each 3° longitude interval was also computed and plotted as red (DT) and blue (ST) lines. A longitude interval was set, as in the horizontal trajectories above.

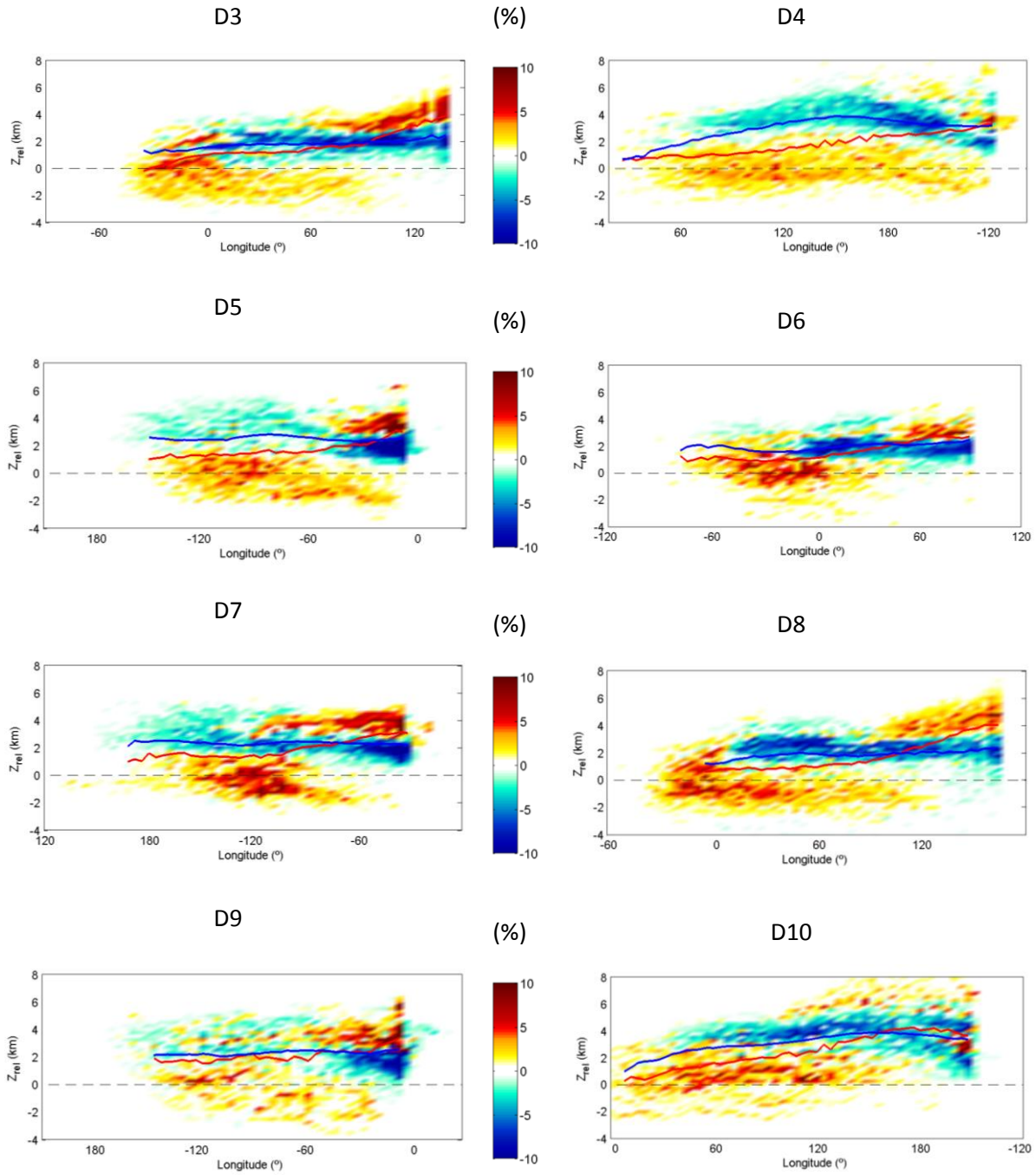

Fig. 13: As in Fig. 12, but for domains D3 through D10.

Looking at figures 12 and 13, it is clear that trajectories in ST events are predominant over trajectories in DT events for relative altitudes around 2-3km. On the other hand, trajectories of DT events are predominant below 2km, extending down to around -2km. This is especially visible for longitudes away from (east of) the release sites. For most domains (excluding domains 1, 4 and 10), DT trajectories are more frequent above 3km in Z_{rel} close to (between 30 and 60° in longitude) the release site. This could be due to the presence of double tropopauses already in these segments of the trajectories. Therefore, excluding the trajectory segments where double tropopauses were already present, we expect this region of higher Z_{rel} in the case of DT events to weaken (or disappear).

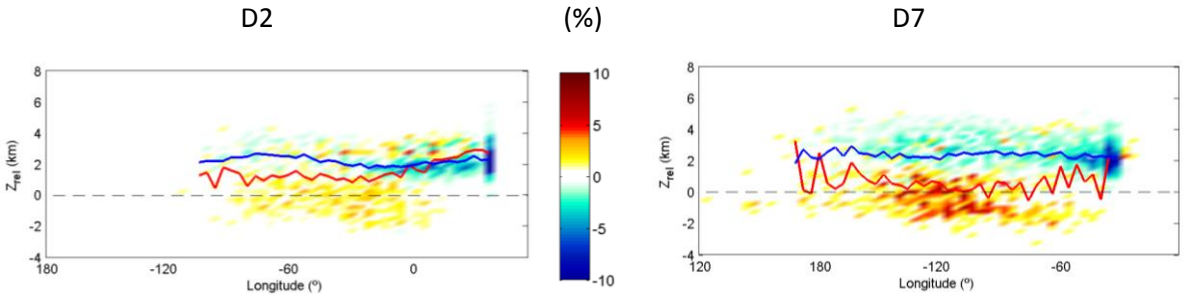

Fig. 14: DT-ST difference between the five-day back-trajectory Z_{rel} probability distribution, between 1980 and 2010, for domains 2 and 7, excluding the segments of the trajectories where DTs were pre-existing. Overlaid is the average Z_{rel} of trajectories for each longitude interval, in red and blue lines for DT and ST events, respectively.

As expected, the higher percentage of DT events above 3km in Z_{rel} near the release site was strongly weakened (in the case of domains 2, shown in Fig. 14 (left), 3 and 4, not shown) or disappeared (for domain 7, shown in Fig. 14 (right), and the rest of the domains, not shown).

Fig. 15 shows the empirical probability density distributions in the longitude-PV phase space, which was divided into 0.2 PVU by 3° longitude bins. These figures were computed to see whether for DT events potential vorticities were lower (and characteristic of tropospheric air) than for ST events. The maps show two relevant features. The differences between density distributions present a discernible degree of zonal homogeneity, and the back-trajectories for DT events are associated with lower mean PV values. The zonal homogeneity should result from the conservation of potential vorticity. For a given ST or DT event the particles change their longitude conserving their PV values. The smaller values of PV in the case of DTs is in agreement with the more southerly flow and lower relative altitude of the retro-trajectories as seen in the previous figures.

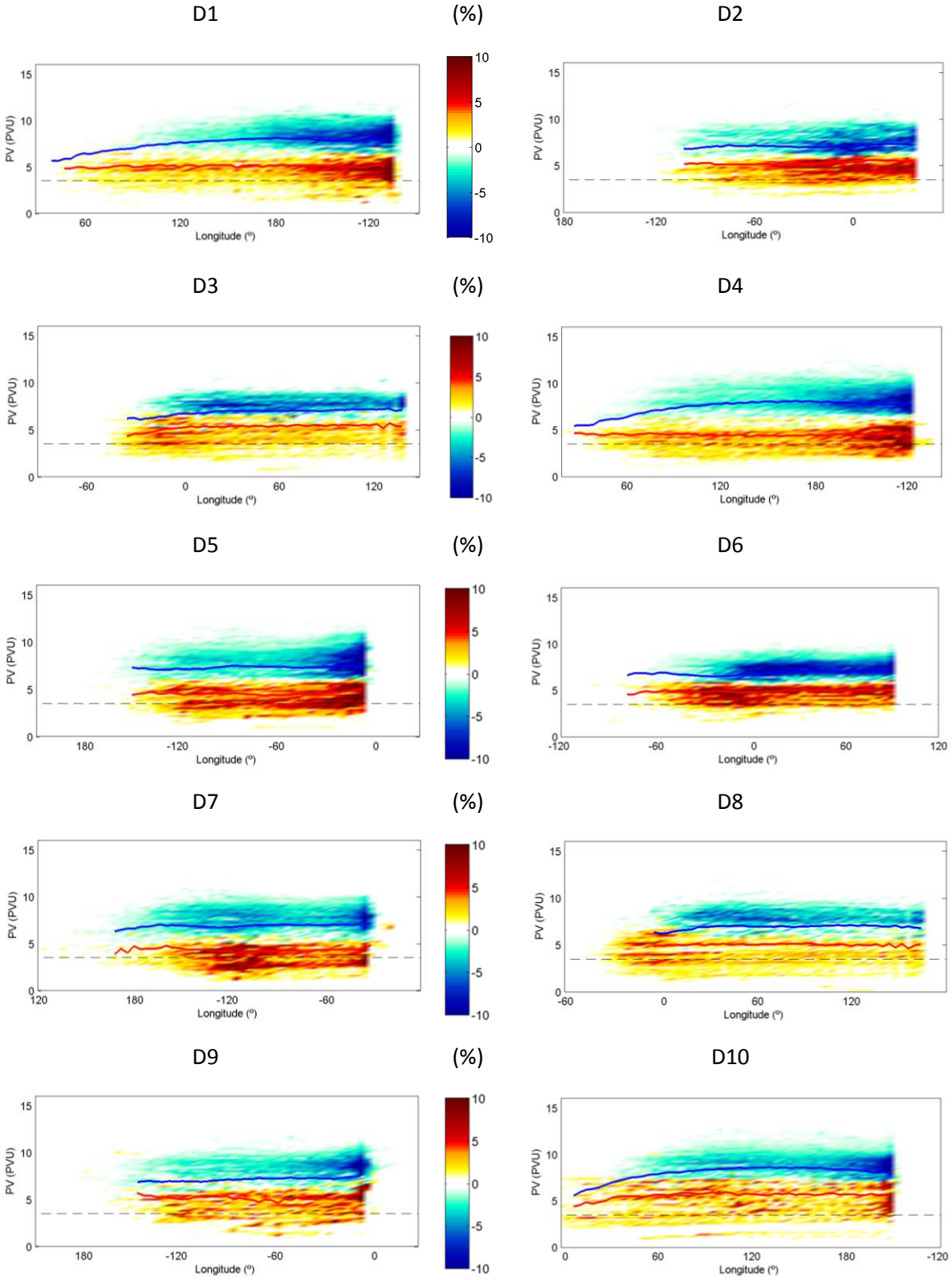

Fig. 15: DT-ST difference between the five-day back-trajectory PV probability distribution, between 1980 and 2010, for domains, D1 through D10. Overlaid is the average PV of trajectories for each longitude interval, in red and blue lines for DT and ST events, respectively. Dashed line is the 3.5 PVU potential vorticity.

Moreover, some cases of DTs are associated with PV values below 3.5 PVU. These cases may result from the intrusion of lower latitude tropospheric air into the lower extratropical stratosphere.

The relative importance of these processes may be assessed by the analysis of the frequency distribution of the mean PV value calculated along the trajectories, shown in the next subsection. This analysis will be complemented with the analysis of other variables: the mean relative altitude and the mean percentage of particles in the troposphere.

3.2.2 Statistics of the trajectory mean variables

The back-trajectories were separated according to the lapse rate structure at the release domains, at the time of arrival, i.e. the back-trajectories were separated into groups associated with either ST or DT events. Each release of particles (the arrival time for back trajectories) was considered as an individual event, and the model's output variables were averaged along the corresponding plume of trajectories, i.e., the means are performed over all particles and over all the instants the back-trajectories were recorded. The following means were calculated: mean relative altitude, Z_{rel}; mean potential vorticity for all particles, PV; mean fraction of particles within the troposphere, TropFract; and mean fraction of particles with potential vorticity below 2PVU, PVFract. Because the relative altitude may change from negative to positive values when the particles go into a double tropopause layer (as seen in the previous subsection), the instants when the centroid trajectory is between double tropopauses were not included in the calculation of the mean relative altitude, $Z_{rel,}$or the fraction of tropospheric particles, TropFract.

Table 2 shows the percentage of trajectories whose mean relative altitude is negative, $Z_{rel} \leq 0$. It also shows the percentage of cases when the fraction of particles, TropFract (i.e. the fraction of particles found below the thermal lapse rate tropopause) exceeds 0.6 or 0.7. The results for these variables are presented for each domain, for ST and DT events.

For every domain, the mean of the mean relative altitude, $\bar{x}\,(Z_{rel})$, for DT events is significantly lower than that of ST events. For some domains the $\bar{x}\,(Z_{rel})$, for DT events is less than half of the $\bar{x}\,(Z_{rel})$ for ST events. Even though $\bar{x}\,(Z_{rel})$ is never below zero, in some domains, the mean of Z_{rel} minus the standard deviation of Z_{rel}, $\bar{x} - \sigma(Z_{rel})$, is negative (for domains 7 and 8).

Table 2: Summary of the results obtained for the ten-day back-trajectories, for each domain and for DT and ST events, including mean relative altitudes ($\bar{x}$) plus and minus the standard deviation of relative altitudes (σ), percentage of negative mean relative altitudes and percentage of fractions of tropospheric air equal or above 0.6 and 0.7.

	Z_{rel} (m)						Z_{rel}≤0 (%)		TropFract ≥0.7 (%)		TropFract ≥0.6 (%)	
	DT			ST			DT	ST	DT	ST	DT	ST
1	337	1690	3044	1929	3283	4480	10,9	1,1	4,7	0,0	8,1	0,1
2	589	1868	3147	1273	2552	3535	9,3	1,1	4,4	0,0	7,0	0,0
3	76	1367	2658	820	2111	3154	17,6	2,6	5,4	0,3	10,5	0,6
4	187	1539	2890	1947	3298	4657	12,5	2,9	5,8	0,3	13,6	1,3
5	142	1442	2743	1554	2855	4149	13,4	2,7	7,2	0,5	13,7	0,6
6	185	1233	2282	1203	2252	3251	13,7	2,8	2,7	0,0	6,6	0,0
7	-53	1338	2729	1147	2538	3877	20,2	5,0	9,6	0,5	18,2	0,9
8	-164	1192	2549	759	2115	3579	22,0	7,4	8,0	0,7	16,6	2,0
9	384	1914	3444	1065	2595	4444	10,3	9,5	6,3	1,4	9,8	2,1
10	437	1798	3159	2073	3434	4738	8,4	2,4	5,3	0,0	5,3	0,1
	$\bar{x}-\sigma$	$\bar{x}$	$\bar{x}+\sigma$	$\bar{x}-\sigma$	$\bar{x}$	$\bar{x}+\sigma$						

This is mirrored in the percentage of centroid trajectories whose mean height is negative, Z_{rel}≤0. For every domain, the percentage of Z_{rel}≤0 is superior in the cases of DT events. Moreover, its maximum is registered for D8, in which 22% of centroid trajectories for DT events had negative mean relative altitude.

This is also reflected in the mean fraction of tropospheric particles, TropFract. In every domain the percentage of DT cases where the mean fraction of tropospheric particles exceeds 0.7 and 0.6 is higher than the percentage of ST cases. In fact, for several domains this percentage is, in the case of ST events, (very close) to zero.

In short, these results show that in the case of DT events, there is a higher percentage of tropospheric particles, with more average trajectories coming from the troposphere, which is also consistent with a mechanism of tropospheric intrusion.

The definition of dynamic tropopause is based on potential vorticity, which is conserved following the motion in adiabatic frictionless flow. In the region of transition between the troposphere and the stratosphere, the PV has a sharp gradient and increases quickly with altitude. Usually the upper threshold used for PV in the troposphere is of 2 PVU. As such, in Table 3, the mean and standard deviation of the mean potential vorticity, $\bar{x}\,(PV)$ and σ(PV) respectively, and the mean

percentage of particles with PV of 2PVU or less, PV≤2PVU, are shown for each domain, for the DT and ST cases.

Table 3: Summary of the results obtained for the ten-day back-trajectories, for each domain and for DT and ST events, including mean potential vorticity ($\bar{x}$) plus and minus the standard deviation of potential vorticity (σ), percentage of particles with potential vorticity equal and under 2PVU, for DT and ST events.

	PV (PVU)						PV≤2PVU (%)	
	DT			ST			DT	ST
1	3,4	5,0	6,6	6,3	7,9	9,6	3,9	0,0
2	3,8	5,2	6,7	5,8	7,1	8,4	1,6	0,0
3	3,7	5,2	6,6	5,7	6,9	8,1	2,7	0,0
4	2,9	4,4	5,9	5,9	7,8	9,7	3,5	0,0
5	3,0	4,4	5,9	5,6	7,4	9,2	2,4	0,1
6	3,7	4,8	6,0	5,7	6,9	8,1	1,1	0,0
7	2,7	4,2	5,7	5,2	6,9	8,6	6,6	0,1
8	3,3	4,9	6,5	5,3	6,9	8,4	4,5	0,3
9	3,4	5,1	6,8	5,3	7,3	9,3	2,9	1,3
10	3,8	5,5	7,3	6,6	8,3	10,0	2,1	0,0
	$\bar{x}-\sigma$	$\bar{x}$	$\bar{x}+\sigma$	$\bar{x}-\sigma$	$\bar{x}$	$\bar{x}+\sigma$		

According to the results displayed in Table 3, for every domain, the mean PV of DT events is significantly lower than the mean PV for ST events. Differences between DT and ST cases range from around 2 to 3 PVU.

Accordingly, there is a decidedly larger mean percentage of particles with PV≤2PVU for DT events than for ST events. In fact, for ST events, the mean percentage of particles with PV≤2PVU is (very close to) zero in nearly every domain at study (with the exception of domain 9).

However, the mean percentage of particles with PV≤2PVU is relatively small, even in the case of DT events, with a maximum of 6.6% in D7. An explanation for these relatively small values can be given by the climatologies of the zonally averaged potential vorticity and first tropopause height for January from 1980 to 2010 (shown in Fig. 16). As shown, the thermal tropopause doesn't coincide with the 2PVU isoline. For the latitudes at study (around 30- 50°N), the PV below the first tropopause could reach up to between 3 and 4 PVU (and was well above 2PVU).

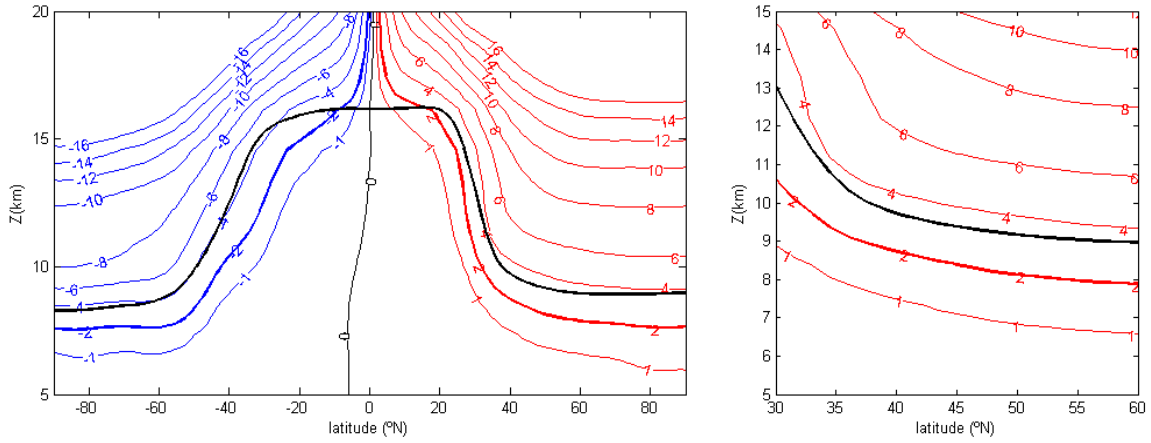

Fig. 16: Zonally averaged potential vorticity (in PVU, red and blue lines) and first tropopause height (black line) climatologies for January, from 1980-2010. The image on the right is a zoom of the image on the left for the latitudes between 30°N and 60°N.

Looking back at Table 3, for the DT events, the values for the mean PV minus the standard deviation of PV, $\bar{x} - \sigma(\text{PV})$, are below 4PVU for every domain at study. In contrast, for ST events, $\bar{\text{x}} - \sigma(\text{ST})$, was above 5PVU in every domain.

In brief, particles have lower potential vorticity values for DT events than for ST events. And for DT events results are still consistent with the presence of tropospheric air between double tropopauses.

Next, these variables will be analyzed in more detail for DT and ST events, using probability distribution functions, histograms and box plots for each domain.

3.2.3 Separating domains into groups

Histograms, box plots and probability density functions were plotted for each domain. However, some of the domains displayed similar behaviour and, therefore, results were arranged into groups of domains. The criteria used to group the domains were based on the percentage of DTs and the location of the domains in the transition region between tropical and extra-tropical tropospauses.

The percentage of DT events was calculated for the original, unfiltered data (Original) and also for the processed data (Filtered), in which DT events were selected according to the separation of ST and DT events (as described in Chapter 2). The results for each domain were plotted in the graphic shown in Fig.17 (top).

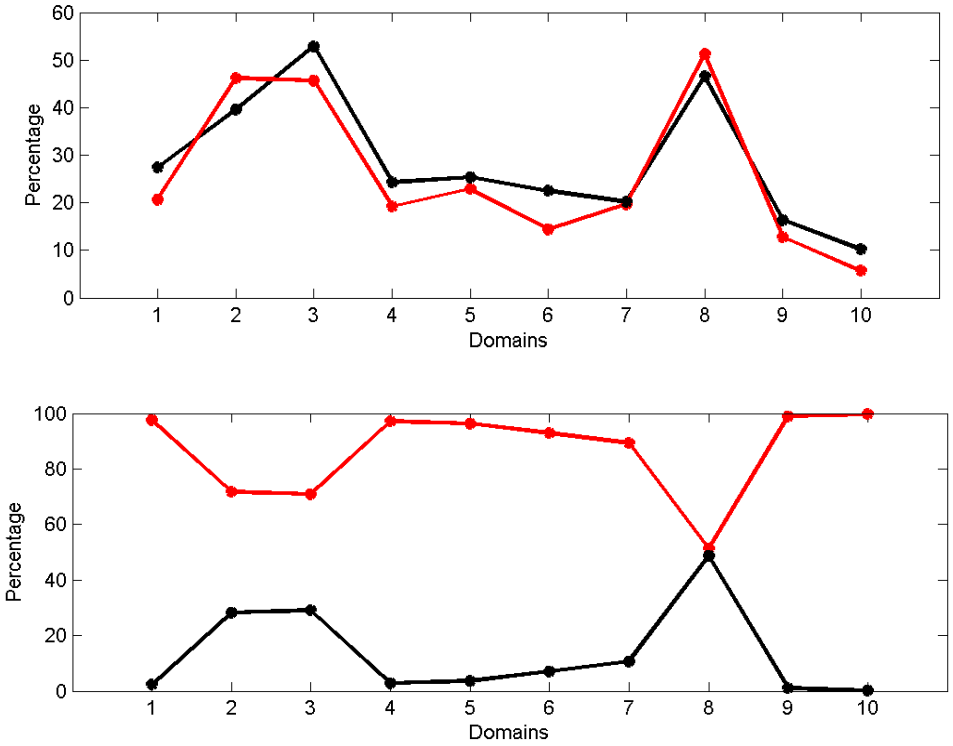

Fig. 17: Percentage of DT events using original data (black) and filtered data (red) for each domain (top). Percentage of extra-tropical (red) and tropical (black) tropopauses for each domain (bottom).

The percentages of first tropopause heights greater and smaller than 13.5km were calculated for each domain. First tropopauses with heights larger than 13.5km are considered tropical tropopauses, and their percentage for each domain was plotted in Fig. 17 (bottom) in black. Whereas tropopauses below 13.5km are labeled extra-tropical tropopauses and their percentage was plotted in red in Fig. 17 (bottom). The 13.5km threshold was suggested by PDFs of the tropopause height, like those shown in Seidel and Randel (2007) or in Randel et al. (2007).

Domains for which the percentage of tropical first tropopauses is relatively high are said to be located in the transition region – region of transition between tropical and extra-tropical tropopauses. Comparing both graphics in Fig. 17, for these domains the percentage of double tropopauses is also relatively high, as expected.

Based on the results shown in Fig. 17, the following groups of domains were defined:

- Group 1 (G1), which includes domains 2, 3 and 8. These domains are located in the transition region and have a high percentage of tropical first tropopauses and DT cases (higher than 1/3 of total cases).

- Group 2 (G2), which includes domains 1, 4, 5, 6 and 7. In these domains the percentage of DT events is lower than for G1 (between 1/3 and 1/5 of total cases) and first tropopauses are mostly extra-tropical.
- Group 3 (G3), which includes domains 9 and 10. For these domains, the percentage of DT cases is very low (less than 1/5 of total cases) and nearly 100% of first tropopauses are extra-tropical.

In addition, temperature profiles were plotted for the point at the center of each domain, using the ERA-Interim data used to run FLEXPART (as described in Chapter 2) for 00, 06, 12 and 18 UTC. The profiles were analyzed in order to confirm that the domains in each group displayed the same behavior, and that different groups displayed different temperature profiles. These temperature profiles were then grouped and are presented in Fig.18.

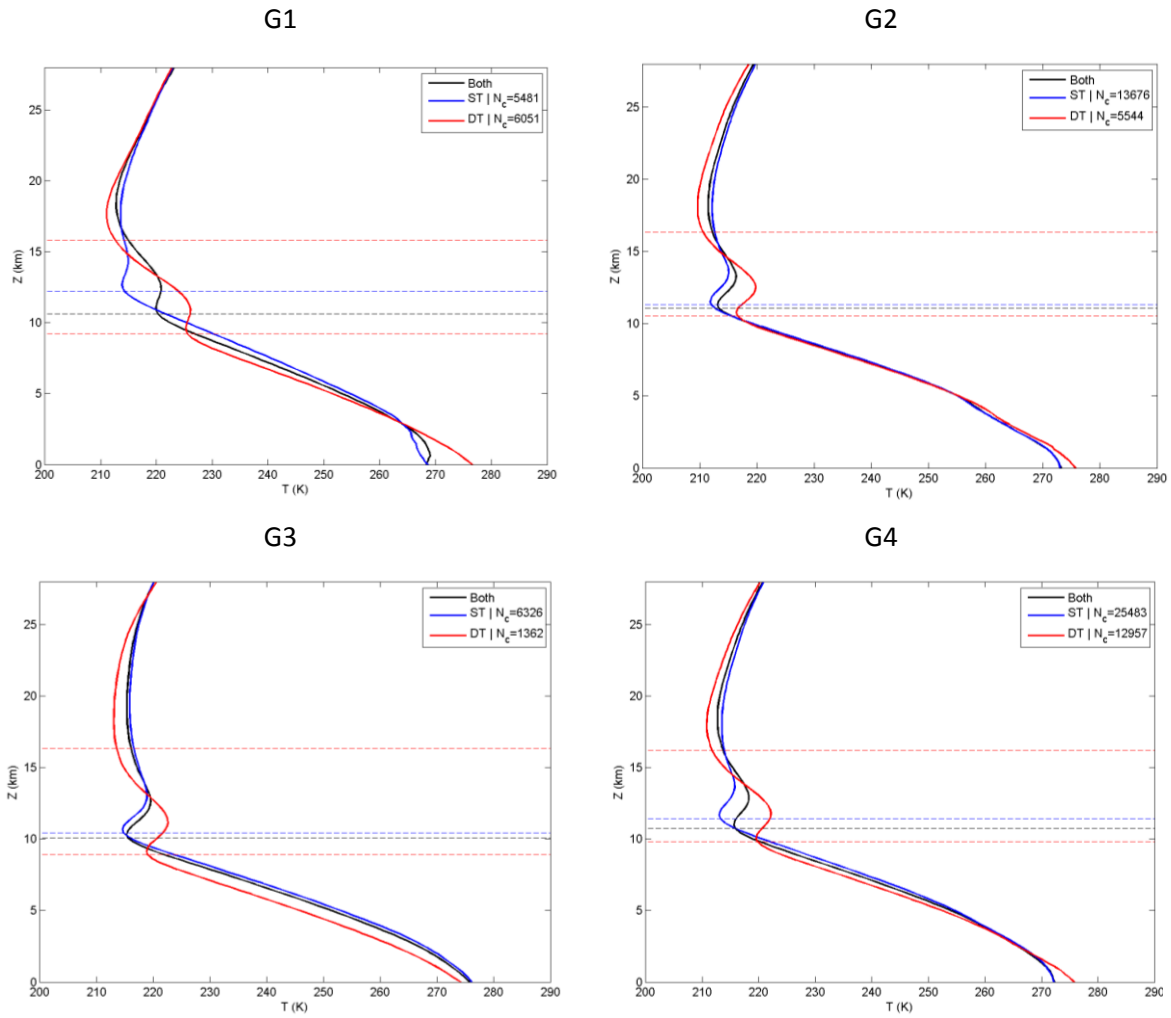

Fig. 18: Temperature profile for grouped domains, G1 through G4, for ST and DT events, and for both types of event together (solid lines). The first and (in the case of DT events) second tropopauses are also shown, as dashed lines, for each case.

According to Fig.18, there are visible differences between ST and DT events, as well as between groups of domains, as expected. In every group of domains, the first tropopause on the case of DT events is lower than the tropopause in ST events. However, the difference between ST and DT events is bigger for G1 (about 3km) and smaller for G2 (around 1km). In accordance, for G1, the temperature at the first tropopause is about 15K higher in the case of DT events, whereas, for G2 it is less than 10K higher.

The results presented in the next pages will be grouped according to groups G1-3, as well as a group, G4, which encompasses every domain considered in this study.

3.2.4 Group of domains 1

Histograms were plotted for the model results of the domains with highest percentage of DT events (higher than 1/3 of cases), with higher percentage of tropical tropopauses: domains 2, 3, 8.

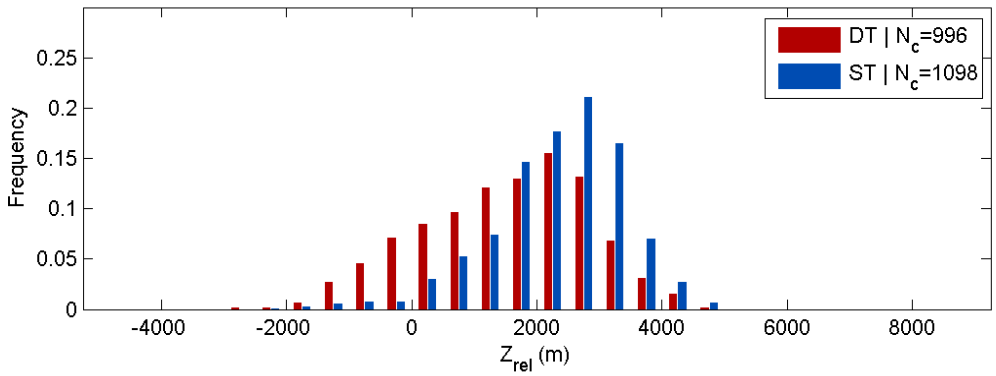

Fig. 19: Relative altitude histogram (fraction) for the mean trajectories in group of domains 1, from 1980 to 2010, separated into ST (blue) and DT (red) events.

Histograms for the relative altitude of the average trajectories (Fig. 19) show that Z_{rel} for DT events are between -2 km and 4km. For ST events the upper and lower limits are about the same, but with a different distribution. For ST events, the Z_{rel} is mostly positive and with the highest fractions centered around 2.5-3.5km. On the other hand, the distribution for DT events shows a considerable percentage of cases with negative Z_{rel}, with higher percentages between 1.5 and 2.5km. These results show that the air arriving at double tropopauses has a lower mean centroid trajectory than the air arriving at single tropopauses.

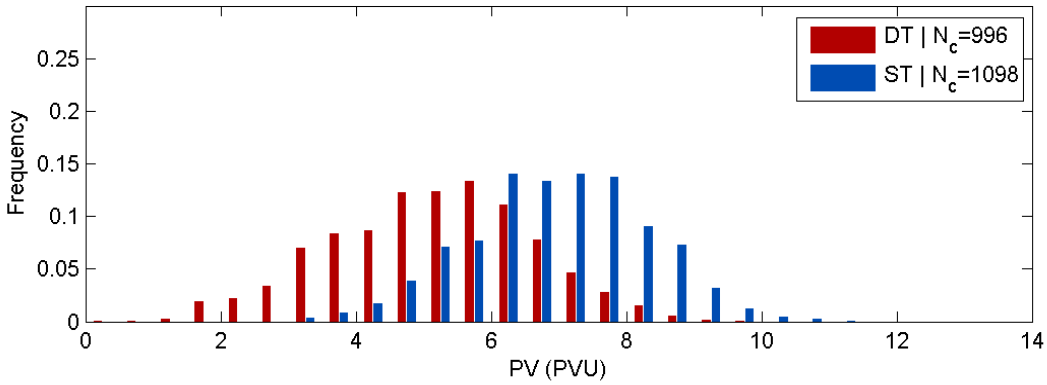

Fig. 20: Potential vorticity histogram (fraction) for the mean trajectories in group of domains 1, from 1980 to 2010, separated into ST (blue) and DT (red) events.

Potential vorticity histograms (Fig. 20) show that, for ST events, PV ranges between 3 and 11 PVU, with larger fractions around 6-8 PVU. In contrast, DT events have PV values between 1 and 9PVU, with higher fractions of cases between 5-6 PVU.

In short, for DT events, relative altitudes and potential vorticity values are, on average, smaller than for ST events. This suggests the presence of more tropospheric air in DT cases, especially with the presence of a slight increase in the distribution of Z_{rel} at around 0km and of PV at between 3 and 4PVU. This is more visible in the probability density function (PDFs) shown in Fig. 21. These PDFs were estimated by the Kernel method (Silverman, 1986) with a normalized Kernel function. The density was evaluated in 100 equally spaced points that cover the range of values in each data set.

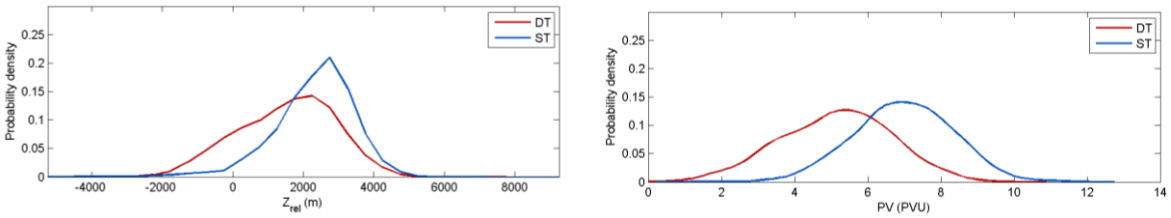

Fig. 21: Probability density function (fraction) for the mean relative altitude, Z_{rel} (left) and mean potential vorticity, PV (right), in group of domains 1, from 1980 to 2010, separated into ST (blue) and DT (red) events.

The Kolmogorov-Smirnov test (K-S test) was used to determine if the datasets for ST and DT events differ significantly. The K-S test (Wilks, 2006) establishes a null-hypothesis, H_0 that the ST and DT datasets belong to the same continuous distribution. This hypothesis is rejected if the discrepancy, D, is high enough.

The K-S test is defined by the equation:

$$D_s = \max\left(|\mathrm{F1}(\mathrm{x}_1) - \mathrm{F2}(\mathrm{x}_2)|\right) \tag{3.1a}$$

In which F1 and F2 are cumulative distribution functions of the variables x_1 and x_2. The hypotheses, H0 is rejected at a α×100% significance level if the following condition is true:

$$D_S > \sqrt{-\frac{1}{2}\left(\frac{1}{n_1}+\frac{1}{n_2}\right)\ln\left(\frac{\alpha}{2}\right)} \tag{3.1b}$$

In which n1 and n2 are the sizes of the x_1 and x_2 datasets. In this work, the test was performed at a 5% significance level.

The K-S tests were performed on the separate data sets for DT and ST events, with results showing that the two types of events have significantly different distributions, at a 5% significance level.

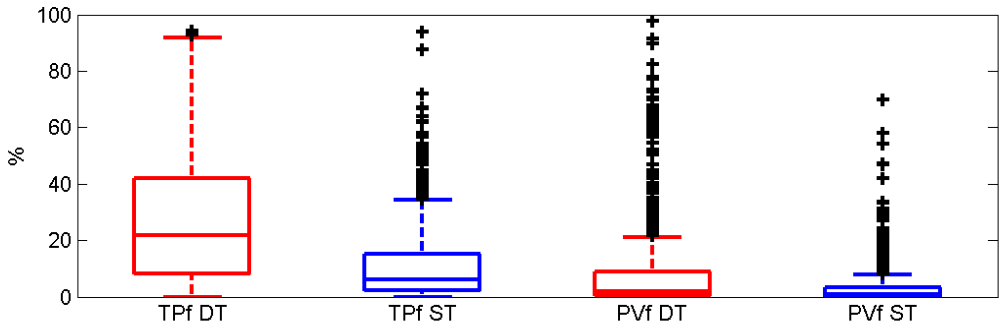

Fig. 22: Box plots for percentage of tropospheric particles and percentage of particles with PV<2PVU, for DT (red and ST (blue) events, for group of domains 1. Plus signs represent the outliers of each distribution.

Finally, box plots (Fig.22) were also plotted for the percentage of tropospheric particles (TPf) and the percentage of particles with PV<2PVU (PVf), for ST and DT events. In these box plots, the central mark is the median, the edges of the box are the 25th and 75th percentiles, the whiskers extend to the most extreme data points that are not considered outliers. The outliers are defined as points at a distance from the 25th and 75th percentile that is larger than 1.5 times the difference between 75th and 25th percentile.

For TPf, it is clear that the percentage of tropospheric particles for DT events is higher than in the case of STs. For DT events, the median TPf is about 20%, while for ST events it was around 10%

(hence, about half of the percentage for DTs). For both cases, the outliers reached up to almost 100%.

For PVf, the percentages for DT events are also clearly higher than for ST events. However, in both cases, the median is close to zero. This is due to the small PV threshold (2 PVU) that is below the thermal tropopause (see Fig. 16). Even though the values of the medians are close to zero, there are appreciable differences: the outliers reach up to 100% in the case of DTs, whereas in the case of ST the maximum percentage reached is about 70%.

3.2.5 Group of domains 2

Histograms were plotted for the model results of the domains with relatively lower percentage (between 1/5 and 1/3) of DTs and tropical tropopauses: domains 1, 4, 5, 6 and 7. For both relative altitudes and potential vorticity, the histograms for ST and DT events seem to be farther apart for this group of domains, G2, than for the previous group, G1. Differences between ST and DT events, therefore, seems more accentuated for this group 2.

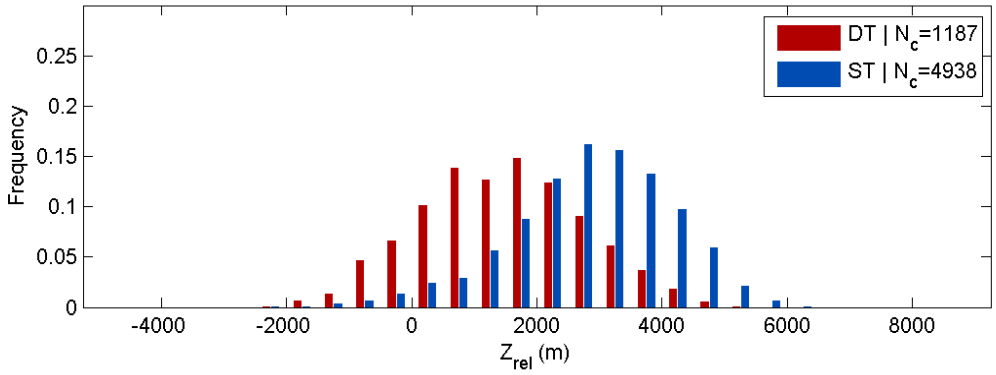

Fig. 23: Relative altitude histogram (fraction) for the mean trajectories in group of group of domains 2, from 1980 to 2010, separated into ST (blue) and DT (red) events.

Histograms for the relative altitude of the average trajectories (Fig. 23) show that for G2, DT events have higher frequency between 0.5 and 2.5km (lower Z_{rel} than in G1). Conversely, ST events peak at around 3 to 4km (which is higher than in G1) and can extend up to over 6km (while, for DT, Z_{rel} only extends up to about 4km. This confirms the idea that air arriving at DTs has, on average, lower altitude than the air arriving at ST events.

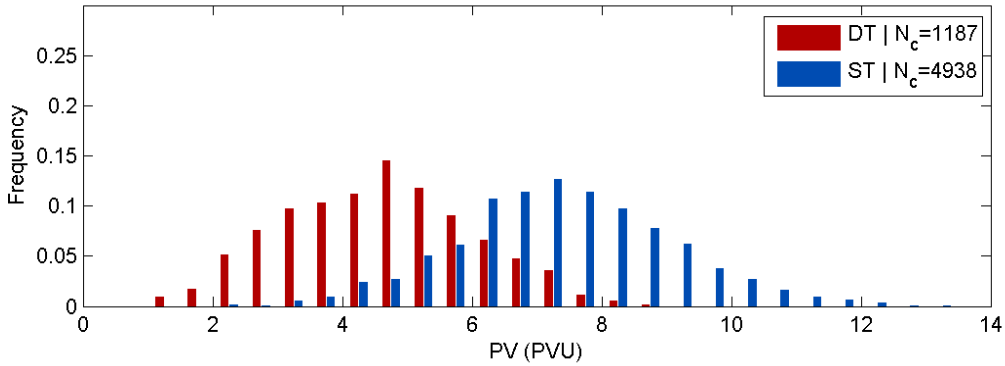

Fig. 24: Potential vorticity histogram (fraction) for the mean trajectories in group of domains 2, from 1980 to 2010, separated into ST (blue) and DT (red) events.

For G2, potential vorticity histograms (Fig. 24) show that for DT events, higher frequencies are observed for PV values between 4 and 5PVU, although they range from 1 to 8PVU, with a considerable fraction of cases where PV is below 4PVU. In contrast, for ST cases, there is only a small percentage of cases with PV below 4PVU. Instead, value range up to 12PVU, and the maximum fractions are observed for 7-8 PVU.

Again, the Z_{rel} for DT cases is visibly smaller, with a larger fraction of negative values, in comparison with ST events. This is not inconsistent with the presence of tropospheric air between double tropopauses, associated with tropospheric intrusions, and is also backed by relatively lower values of PV for DT events, including the relatively higher fraction of cases in which PV is smaller than 4PVU.

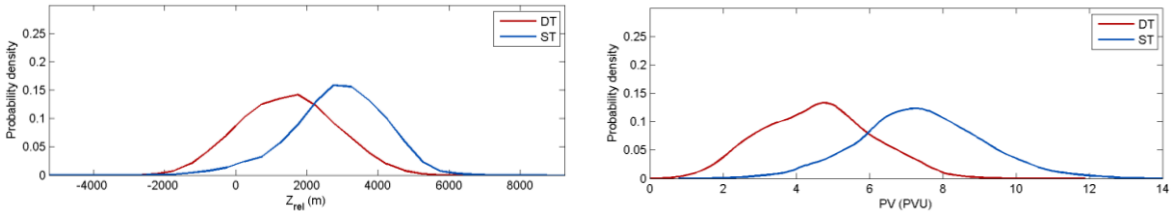

Fig. 25: Probability density function (fraction) for the mean relative altitude, Zrel (left) and mean potential vorticity, PV (right), in group of domains 2, from 1980 to 2010, separated into ST (blue) and DT (red) events.

The probability density functions (Fig. 25) for these distributions show the shift to lower values of Z_{rel} and PV, for DT events when compared with ST events. This shift was also observed (to some extent) for G1. However, for G2, the Z_{rel} distributions are both unimodal, while the PV distribution for DT cases appears to have a region of higher probability density around 3-4PVU (in addition to the maximum observed at around 5PVU).

The K-S tests performed on DT and ST data sets showed that distributions of Z_{rel} and PV are significantly different for DT and ST cases, for this group of domains as well.

Looking at the box plots (Fig. 26) for TPf and PVf, it is apparent (even more so than in G1) that DT events have a much larger percentage of tropospheric particles, in comparison with ST events. In particular, the median of the TPf for DT cases stands at nearly 30%, with outliers reaching up to 100%. On the other hand, for ST cases TPf stays at about 5% with outliers up to about 90%. In addition, the median of PVf for DT cases is also visibly larger than for ST cases, whose median is very close to zero. In short, these results are also not against the mechanism of tropospheric intrusion in the stratosphere during DT cases.

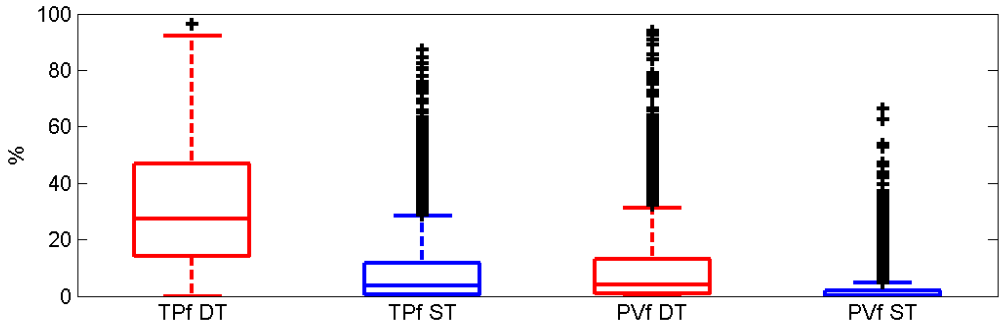

Fig. 26: Box plots for percentage of tropospheric particles and percentage of particles with PV<2PVU, for DT (red and ST (blue) events, for group of domains 2. Plus signs represent the outliers of each distribution.

3.2.6 Group of domains 3

Histograms were plotted for the model results of the domains with lowest percentage (less than 1/5) of DTs and tropical tropopauses: domains 9 and 10.

Histograms for the relative altitude of the average trajectories (Fig. 27) show that for G3, histograms for DT and ST events are closer together than in G2 and the histogram for DT loses its unimodality seen in G2. Furthermore, for these domains, for negative relative altitudes, both DT and ST events have low fractions. However, for low but positive values of Z_{rel} (for Z_{rel} under 3km), the fractions of DT are higher, while for Z_{rel} over 3km the fractions of ST events are higher. Therefore, there is still a difference in the distribution of Z_{rel} for the two different types of events, in which DT events have mean trajectories with lower relative altitudes than ST events.

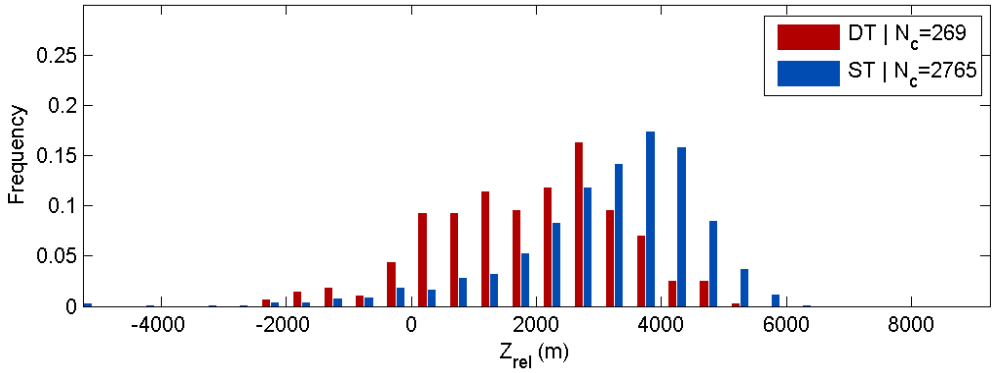

Fig. 27: Relative altitude histogram (fraction) for the mean trajectories in group of domains 3, from 1980 to 2010, separated into ST (blue) and DT (red) events.

Conversely, for DT events, the distribution of PV (Fig. 28) is about 3PVU lower than for ST events. The distribution of PV for DT cases has a maximum around 5PVU with smaller maxima around 3PVU and 7PVU, while for ST there is one single maximum, centred at around 8PVU.

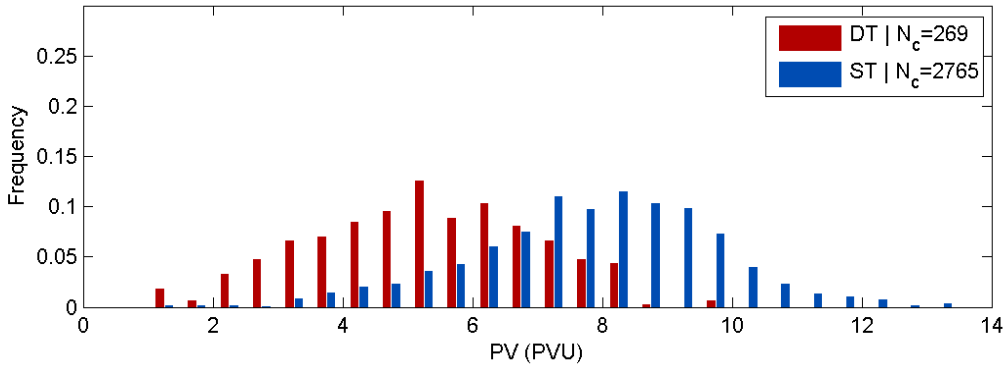

Fig. 28: Potential vorticity histogram (fraction) for the mean trajectories in group of domains 3, from 1980 to 2010, separated into ST (blue) and DT (red) events.

This is reflected in the probability density functions (Fig. 29), where the distributions for DT events are concentrated on lower values of both Z_{rel} and PV than the distributions for ST events. For this group of domains, the K-S test also shows that the ST and DT events have significantly different distributions of PV and Z_{rel}.

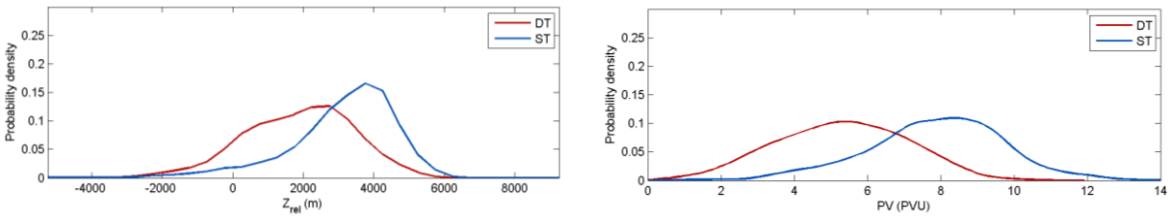

Fig. 29: Probability density function (fraction) for the mean relative altitude, Z_{rel} (left) and mean potential vorticity, PV (right), in group of domains 3, from 1980 to 2010, separated into ST (blue) and DT (red) events.

For this group of domains, percentages are in general smaller but the difference between DT and ST events is still apparent (Fig. 30). For G3, as in G1 and G2, the percentage of tropospheric particles, using both the thermal lapse rate tropopause and the dynamical tropopause, is higher for DT events, in tune with the Z_{rel} and PV distributions and the occurrence of tropospheric intrusions. For ST events, the median TPf and PVf are, for these domains, very close to zero.

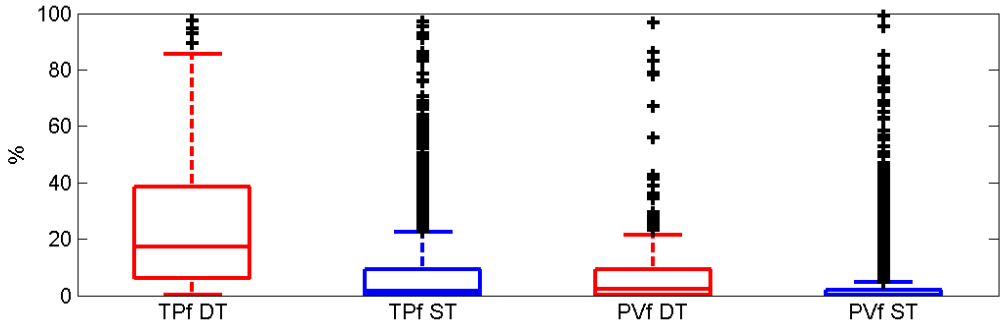

Fig. 30: Box plots for percentage of tropospheric particles and percentage of particles with PV<2PVU, for DT (red and ST (blue) events, for group of domains 3. Plus signs represent the outliers of each distribution.

3.2.7 Grouped domains

Histograms were plotted for the model results of every domain: 1-10, in order to get a global view of the differences between the distributions for DT and ST events.

Globally, the distribution of relative altitudes (Fig. 31) of mean centroid trajectories for DT events shifts towards lower values when compared to the distribution for ST events. Distributions for DT events have bigger fractions for Z_{rel} below 2.5km and smaller fractions than ST events for Z_{rel} above 2.5km. Therefore, particles arriving between DTs are coming from lower altitudes, in relation to the tropopause, that is, from the high troposphere and from the lower stratosphere.

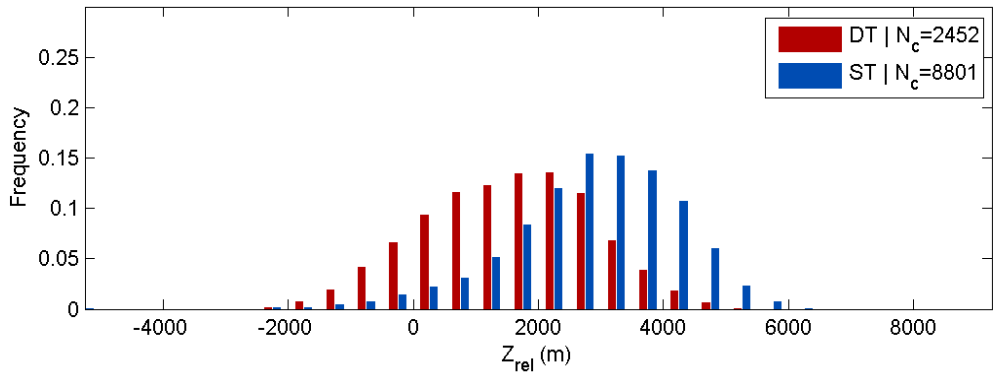

Fig. 31: Relative altitude histogram (fraction) for the mean trajectories in group of domains 4, from 1980 to 2010, separated into ST (blue) and DT (red) events.

Globally, the distribution of potential vorticity (Fig. 32) of mean centroid trajectories for DT events also tends towards lower values than the distribution for ST events. DT events have a greater fraction of PV below 6PVU than ST events, with a considerable fraction of DT cases in which PV is below 4PVU. In general, DT events have PV values between 1 and 9 PVU (with a very small fraction of PV values over 8PVU). On the other hand, ST events have a greater fraction of cases with PV over 6PVU, including a considerable fraction of cases with PV over 8PVU.

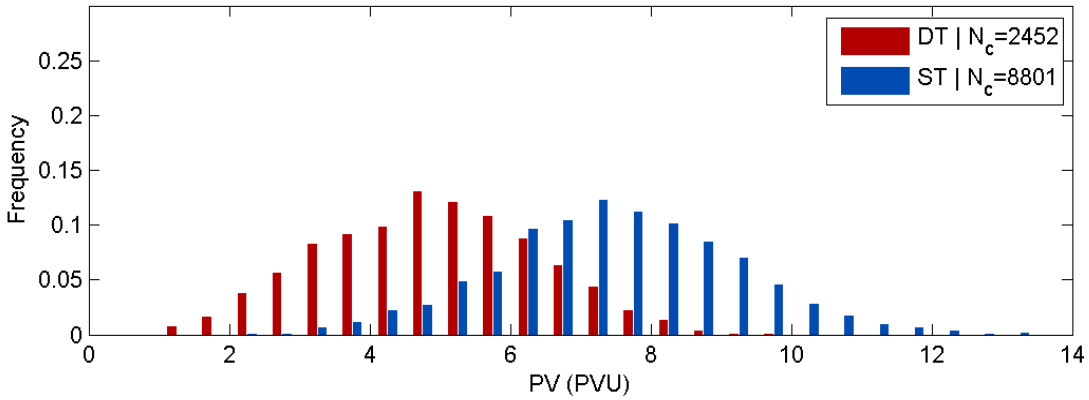

Fig. 32: Potential vorticity histogram (fraction) for the mean trajectories in group of domains 4, from 1980 to 2010, separated into ST (blue) and DT (red) events.

Probability density functions (Fig. 33) for DT and ST events have almost the same lower boundaries (-2km for Z_{rel} and 1PVU for PV), but different upper boundaries. For DT events, the upper boundaries of the density distributions are much lower than for ST events (about 2km lower for Zrel and about 3PVU for PV distributions).

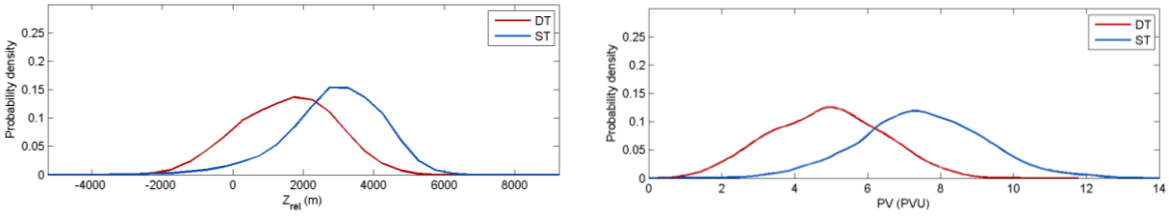

Fig. 33: Probability density function (fraction) for the mean relative altitude, Z_{rel} (left) and mean potential vorticity, PV (right), in group of domains 4, from 1980 to 2010, separated into ST (blue) and DT (red) events.

As expected, for the grouped domains, the distributions of Z_{rel} and PV for DT and ST events are significantly different at the 5% significance level, according to the performed K-S test.

Globally, the box plots (Fig. 34) show that DT events have a higher percentage of tropospheric particles. This supports the hypothesis that the development of double tropopauses might be

related with tropospheric intrusions, and that tropospheric intrusions might be a contributing mechanism in their formation.

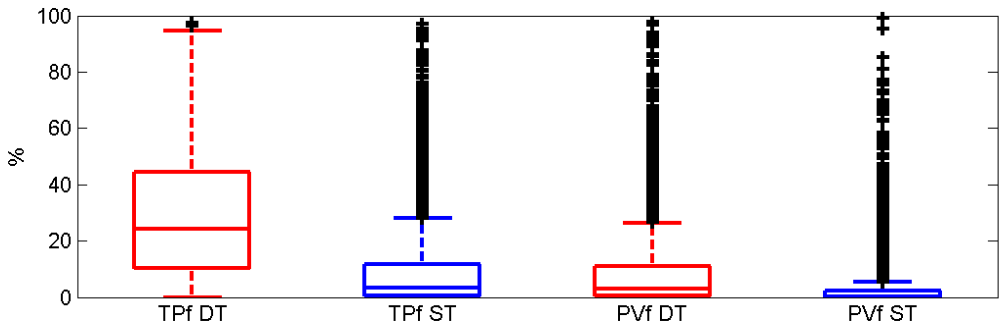

Fig. 34: Box plots for percentage of tropospheric particles and percentage of particles with PV<2PVU, for DT (red and ST (blue) events, for group of domains 4. Plus signs represent the outliers of each distribution.

3.2.8 Concluding remarks

In conclusion, the results produced by the FLEXPART runs for the month of January, from 1980 to 2010, for the domains at study show that the air that is found between double tropopauses is originated at lower latitudes in the five days prior to arrival. This is observed for every domain and can be seen through the trajectory probability density, as well as through the average latitude for each longitude.

It was also shown that, for the air between double tropopauses, mean trajectories have lower relative altitudes, with a lower mean relative altitude, as well as a higher percentage of mean trajectories with a negative relative altitude. This means that the air between double tropopauses is sometimes originated below the tropopause. This is supported by the higher percentage of tropospheric particles between double tropopauses.

In addition, it was shown that for the air between double tropopauses, mean trajectories have lower potential vorticity values, with a higher percentage of particles with potential vorticity lower than 2PVU, as well as a higher fraction of cases in which the potential vorticity is below 4PVU.

Although there are variations between domains and also variations between groups of domains, these conclusions are shared by every domain and group of domains at study, as well as by a global domain which includes every individual domain.

These conclusions support the idea that intrusions of tropical tropospheric air into the lower extratropical stratosphere make a significant contribution for the occurrence of double tropopauses. However, results show that, more frequently, the tropospheric air does not seem to be the main component in the air between double tropopauses, which suggests that other mechanisms apart from tropospheric intrusions are at play.

Chapter 4. Conclusion

In conclusion, the occurrence of multiple tropopauses is a common feature in mid-latitudes, especially during the winter season. Due to their importance in the exchanges between stratosphere and troposphere, the structure and variability of multiple tropopauses have been the subject of several studies in recent years. However, a significant level of uncertainty in this topic remains, most notably when it comes to the origin of the air between tropopauses and the mechanism leading to the formation and development of double tropopauses.

This thesis' goal was to study the origin of air between double tropopauses, through the study of the dynamic characteristics of the air between double tropopauses. This was attempted by using a Lagrangian particle dispersion model, FLEXPART.

This model was tested using multiple tropopause events recorded in literature. Results obtained for three test cases (in Part 1 of Chapter 3) suggest that FLEXPART is sensitive to the occurrence of double tropopause events. As such, this model was used in this work to study the climatological origin of air between double tropopauses.

The results produced by FLEXPART's backward runs (in Part 2 of Chapter 3) for the month of January, from 1980 to 2010, for several locations (domains) at study showed that the air that is found between double tropopauses is originated at lower latitudes and relative altitudes in the five days prior to arrival. This was observed for every domain and was also seen through the trajectory probability density, and through the average latitude and relative altitude for each longitude.

For air between double tropopauses, it was shown (using histograms, probability density functions and box plots) that mean trajectories tend to have lower relative altitudes (with a higher fraction of negative relative altitudes) and lower values of potential vorticity (with a higher fraction of potential vorticity below 4PVU). These results are consistent with the idea that double tropopauses are frequently associated with tropospheric intrusions, which is supported by the higher percentage of tropospheric particles between double tropopauses, using both the thermal lapse rate and dynamic definitions of tropopause. In fact, in a large fraction (about 30%) of the analyzed DT events, the air moving towards the DT layer has tropical or sub-tropical characteristics with PV values below 4PVU. Moreover, in a large fraction (around 20%) of the DT events more than half of the air particles which move towards the DT layer were found in the

troposphere, i.e., below the lapse rate tropopause. Using the January climatologies of the zonally averaged PV and of the zonally averaged height of the first tropopause as reference (Fig. 16), the global results of this study (see Figs. 9-11, 32 and 34) may be summarized as follows. The air that reaches the region between DTs comes predominantly from upper tropical troposphere or from a layer just above the tropopause, whereas, in the case of ST events, the air that reaches the same spatial domains comes predominantly from the lower extratropical stratosphere. In fact, for more than 75% of the analysed DT events the mean PV is below 6 PVU. In contrast, the air that reaches the same spatial domains has mean PV above 7 PVU (a clear stratospheric value) for more than 60% of the ST events. Moreover, in about 75% (50%) of the DT events at least 10% (25%) of air particles were found in the troposphere, i.e., below the lapse rate tropopause, whereas in over 70% (50%) of the ST events more than 90% (95%) the air particles were found in the stratosphere, i.e., above the lapse rate tropopause.

In conclusion, our results show that the poleward excursions of subtropical and tropical air accompanied by tropospheric intrusions into the lower extratropical stratosphere are one of the main mechanisms for the occurrence of double tropopause structures.

References

Añel, J. A., Antuña, J. C., de la Torre, L., Nieto, R. and Gimeno, L. (2007). Global statistics of multiple tropopauses from the IGRA database. Geophys. Res. Lett., 34, L06709.

Añel, J. A., Antuña, J. C., de la Torre, L., Castanheira, J. M. and Gimeno, L. (2008). Climatological features of global multiple tropopause events. J. Geophys. Res., 113, D00B08.

Añel, J. A., de la Torre, L. and Gimeno, L. (2012). On the origin of the air between multiple tropopauses at midlatitudes. The Scientific World Journal, Volume 2012, 191028, 5pgs.

Baldwin, M. P. and Dunkerton, T. J. (1999). Downward propagation of the Arctic Oscillation from the stratosphere to the troposphere. J. Geophys. Res., 104, 30,937– 30,946.

Baldwin, M. P. and Dunkerton, T. J. (2001). Stratospheric harbingers of anomalous weather regimes. Science, 294, 581 – 584.

Berthet, G., Esler, J. G. and Haynes, P. H. (2007). A Lagrangian perspective of the tropopause and the ventilation of the lowermost stratosphere. J. Geophys. Res., 112, D18102.

Bethan, S., Vaughan, G. and Reid, S. J. (1996). A comparison of ozone and thermal tropopause heights and the impact of tropopause definition on quantifying the ozone content on the troposphere. Q. J. R. Meteorol. Soc., 122, 929– 944.

Birner, T. (2006). Fine-scale structure of the extratropical tropopause region. J. Geophys. Res., 111, D04104.

Birner, T. (2010). Recent widening of the tropical belt from global tropopause statistics: Sensitivities. J. Geophys. Res., 115, D23109.

Castanheira, J. M. and Gimeno, L. (2011). Association of double tropopause events with baroclinic waves. J. Geophys. Res., 116, D19113.

Castanheira, J. M., Peevey, T. R., Marques, C. A. F. and Olsen, M. A. (2012). Relationships between Brewer-Dobson circulation, double tropopauses, ozone and stratospheric water vapour. Atmos. Chem. Phys., 12, 10195–10208.

Dorling, S. R., Davies, T. D. and Pierce, C.E. (1992). Cluster analysis: a technique for estimating the synoptic meteorological controls on air and precipitation chemistry - method and applications. Atmos.Environ., 26A, 2575–2581.

Flesch, T. K., Wilson, J. D. and Lee, E. (1995). Backward-time Lagrangian stochastic dispersion models and their application to estimate gaseous emissions. J. Appl. Meteorol., 34, 1320–1333.

Gettelman, A., Geller, M. A. and Haynes, P. H. (2007). A SPARC tropopause initiative. SPARC Newsl., 29, 14– 20.

Haynes, P., Scinocca, J. and Greenslade, M. (2001). Formation and maintenance of the extratropical tropopause by baroclinic eddies. Geophys. Res. Lett., 28(22), 4179– 4182.

Held, I. (1982). On the height of the tropopause and the static stability of the troposphere. J. Atmos. Sci., 39, 412– 417.

Holton, J. R., Haynes, P. H., McIntyre, M. E., Douglass, A. R., Rood, R. B. and Pfister, L. (1995). Stratosphere-troposphere exchange, Rev. Geophys., 33, 403– 439.

Hoskins, B. J., McIntyre, M. E. and Robertson, A. W. (1985). On the use and significance of isentropic potential vorticity maps. Q. J. R. Meteorol. Soc., 111, 877–946.

Kochanski, A. (1955). Cross sections of the mean zonal flow and temperature along 80. W. J. Meteor., 12, 95–106.

Limpasuvan, V. And Hartmann, D. L. (2000). Wave-Maintained Annular Modes of Climate Variability. J. Climate, 13, 4414–4429.

Olsen, M. A., Douglass, A. R., Newman, P. A., Gille, J. C., Nardi, B., Yudin, V. A., Kinnison, D. E. and Khosravi, R. (2008). HIRDLS observations and simulation of a lower stratospheric intrusion of tropical air to high latitudes. Geophys. Res. Lett., 35, L21813.

Pan, L. L., Randel, W. J., Gille, J. C., Hall, W. D., Nardi, B., Massie, S., Yudin, V., Khosravi, R., Konopka, P. and Tarasick, D. (2009). Tropospheric intrusions associated with the secondary tropopause. J. Geophys. Res., 114, D10302.

Peevey, T. R., Gille, J. C., Randall, C. E. and Kunz, A. (2012). Investigation of double tropopause spatial and temporal global variability utilizing High Resolution Dynamics Limb Sounder temperature observations. J. Geophys. Res., 117, D01105.

Randel, W. J., Seidel, D. J. and Pan, L. L. (2007). Observational characteristics of double tropopauses, J. Geophys. Res., 112, D07309.

Reichler, T., Dameris, M. and Sausen, R. (2003). Determining the tropopause height from gridded data. Geophys. Res. Lett., 30(20), 2042.

Reid, G. C. and Gage, K. S. (2006). The tropical tropopause over the western Pacific: Wave driving, convection, and the annual cycle. J. Geophys. Res., 101, D16, 21233-21241.

Schneider, T. (2004). The tropopause and the thermal stratification in the extratropics of a dry atmosphere. J. Atmos. Sci., 61, 1317– 1340.

Schneider, T. and Sobel, A. H. (2007). The Global Circulation of the Atmosphere. Princeton University Press. 400pp.

Seibert, P. and Frank, A. (2004). Source-receptor matrix calculation with a Lagrangian particle dispersion model in backward mode. Atmos. Chem. Phys., 4, 51–63.

Seidel, D. J., and Randel, W. J. (2007). Recent widening of the tropical belt: Evidence from tropopause observations. J. Geophys. Res., 112, D20113.

Shepherd, T. G. (2002). Issues in stratosphere-troposphere coupling, J. Meteorol. Soc. Jpn., 80(4B), 769– 792.

Silverman B. W. (1986). Density Estimation for Statistics and Data Analysis. Chapman and Hall: London, 175 pp.

Stohl, A., Eckhardt, S., Forster, C., James, P., Spichtinger, N. and Seibert, P. (2002). A replacement for simple back trajectory calculations in the interpretation of atmospheric trace substance measurements. Atmos. Environ., 36, 4635–4648.

Stohl, A., et al. (2003). Stratosphere-troposphere exchange: A review, and what we have learned from STACCATO. J. Geophys. Res., 108(D12), 8516.

Stohl, A., Forster, C., Frank, A., Seibert, P. and Wotawa, G. (2005). Technical note: The Lagrangian particle dispersion model FLEXPART version 6.2. Atmos. Chem. Phys., 5, 2461-2474.

Thompson, D. W. J., Baldwin, M. P. and Wallace, J. M. (2002). Stratospheric connection to Northern Hemisphere wintertime weather: Implications for prediction. J. Clim., 15, 1421 - 1428.

Thuburn, J. and Craig, G. C. (2002). On the temperature structure of the tropical substratosphere. J. Geophys. Res., 107(D2), 4017, 2001JD000448.

Wang, S. and Polvani, L. M. (2011). Double tropopause formation in idealized baroclinic life cycles: The key role of an initial tropopause inversion layer, J. Geophys. Res., 116, D05108.

Wilks, D. S. (2006). Statistical Methods In Atmospheric Sciences. Elsevier, 649 pp.

World Meteorological Organization (WMO) (1957). “Meterology: a three dimensional science,” WMO Bulletin, vol. 6, pp. 134–138.